buildings

MDPI

Article

EVCrane: An Evolutionary Optimization Framework for Mobile Crane Repositioning and Integrated Logistics Route Planning

Wittaya Srisomboon [1] and Narongrit Wongwai [2,*]

[1] Faculty of Science and Engineering, Kasetsart University, Chalermphrakiat Sakon Nakhon Province Campus, Sakon Nakhon 47000, Thailand; fsewys@ku.ac.th
[2] Faculty of Engineering at Sriracha, Kasetsart University, Sriracha Campus, Chonburi 20230, Thailand
* Correspondence: narongrit@eng.src.ku.ac.th; Tel.: +66-909847336

Abstract

Mobile crane repositioning and on-site logistics coordination constitute a highly coupled, nonlinear decision problem in constrained construction environments. Existing approaches largely decouple these tasks, limiting achievable system-level efficiency. This study introduces EVCrane, a kinematics-informed evolutionary optimization framework that simultaneously optimizes crane stopping positions, stockpile deployment, and task allocation within a unified mixed continuous–binary formulation. Unlike distance-based approximations, the proposed model propagates geometric decisions through coordinated crane motion components—including radial boom adjustment, slewing rotation, and vertical hoisting—ensuring physically consistent cycle-time estimation. A real industrial case study was used to benchmark five optimization algorithms under identical MATLAB R2026a implementations. The Genetic Algorithm (GA) achieved the lowest total crane engaged time (34.516 h), reducing operational duration by 6.45% and utilization cost by 6.32% compared with a deterministic nonlinear programming baseline. Comparative analysis reveals that recombination-based evolutionary search exhibits superior compatibility with assignment-driven non-convex landscapes, outperforming swarm-based and trajectory-based alternatives. Sensitivity analysis confirms structural robustness of optimal spatial configurations under parametric perturbations. The proposed framework advances crane planning from decoupled geometric heuristics toward integrated, physics-consistent, and computationally robust optimization, supporting intelligent and sustainable construction site management.

Keywords: mobile crane repositioning; construction logistics optimization; multi-objective optimization; evolutionary algorithms; hybrid metaheuristic; spatial constraints

Check for updates

Academic Editors: David Arditi and Salvatore Antonio Biancardo

Received: 1 March 2026
Revised: 10 April 2026
Accepted: 16 April 2026
Published: 18 April 2026

Copyright: © 2026 by the authors. Licensee MDPI, Basel, Switzerland. This article is an open access article distributed under the terms and conditions of the Creative Commons Attribution (CC BY) license.

1. Introduction

Mobile cranes are indispensable in high-rise construction because they enable lifting and positioning of heavy components, prefabricated elements, and materials in constrained urban environments. However, high-rise sites typically exhibit limited maneuvering space, dense temporary facilities, and complex traffic interactions among equipment and supply vehicles. Under such conditions, mobile crane repositioning (i.e., selecting feasible stopping points and sequencing relocations) and logistics route planning (i.e., routing trailers/vehicles within the site) can strongly influence operational productivity, cost efficiency, and environmental performance. When these decisions are handled sub-optimally,

projects may experience excessive crane walking distance, longer lifting cycles, increased congestion, and higher fuel use, ultimately degrading project performance.

Recent studies show that planning and optimization in construction increasingly emphasize site-level decision-making (e.g., facility layout, routing, and equipment operations), yet the operational reality remains difficult: the decision space is often nonlinear, discontinuous, and mixed-variable, where feasibility depends on kinematic limits, boundary constraints, collision risks, and route connectivity. For example, research on crane walking–involved lift operations highlights how obstacle-rich environments require algorithmic planning methods inspired by robotics to generate feasible walking plans under congestion and limited paths [1]. Similarly, automated lift path planning for cranes using environmental point clouds indicates that practical lift planning must account for rich geometric constraints and collision checking, reinforcing the need for advanced computational planning rather than rule-of-thumb layouts [2].

Parallel to crane operation planning, the construction site layout planning (CSLP) literature has progressed rapidly because layout decisions determine material handling distance, safety exposure, and workflow efficiency. In 2023–2024, studies have emphasized (i) mapping CSLP knowledge structures and parameters, and (ii) developing multi-objective or constraint-aware models. For instance, a social network analysis of CSLP in Buildings synthesizes critical parameters and interrelationships, providing evidence that layout performance is driven by intertwined decisions rather than isolated facility placements [3]. In addition, studies have proposed mathematical modeling approaches for integrated construction site planning, including mechanisms and temporary facilities, demonstrating the trend toward more formalized site-level optimization [4]. Practical algorithmic development continues as well: GA-based models have been reported for optimizing site layout in building projects, illustrating the relevance of evolutionary search to complex planning problems [5]. A GA-based CSLP model further incorporates traveling distance cost and safety relationships, underscoring that modern CSLP formulations increasingly treat safety and operational efficiency jointly [6].

Beyond CSLP, construction research has increasingly examined optimization under uncertainty, sustainability, and resource constraints. For example, hybrid simulation–metaheuristic approaches have been used to reduce greenhouse gas emissions by jointly considering project activities and resource transportation, which is aligned with the growing expectation that construction optimization should deliver environmental benefits—not only time/cost savings [7]. Furthermore, "lessons learned" analyses in CSLP emphasize that many studies still rely on fabricated or simulated data, and they call for more realistic planning assumptions and transferable decision frameworks for diverse project contexts.

Meanwhile, logistics planning and routing—well studied in operations research—has been increasingly contextualized to construction supply chains, prefabrication, and on-site delivery coordination. In 2024, Yang et al. study on data-driven logistics collaboration for prefabricated supply chains with multiple factories reflects this shift toward multi-echelon coordination, data-driven collaboration, and operational optimization in construction logistics systems [8]. In 2025, Tetik et al. proposed a study on construction logistics capacity alignment through simulation further demonstrates how simulation can support logistics planning decisions at scale [9]. Complementary research proposes IT artifacts such as a Construction Logistics Control Tower to coordinate logistics activities across the supply chain, revealing an emerging direction toward platform-based logistics optimization and decision governance [10]. The supply-chain dimension of construction is also expanding in Buildings-focused literature; for example, 2024 bibliometric analysis maps supply chain management research within modular integrated construction, highlighting the growing role of coordinated logistics and complex project management [11].

Within the optimization-methods landscape, recent CSLP and construction planning studies highlight two major patterns: (i) metaheuristics remain central for complex nonconvex planning problems, and (ii) there is a growing emphasis on multi-objective and safety-aware formulations. In 2024, Borges et al. presents a hybrid framework for multi-objective CSLP optimization and discusses the scaling challenges of increasingly complex formulations [12]. In 2025, a researcher proposed CSLP as a quadratic assignment problem and proposes an advanced metaheuristic, reinforcing the continued interest in metaheuristics as practical solvers for large search spaces [13]. In 2025, Pham et al. proposed a dynamic Mult objective CSLP model for prefabricated construction emphasizing efficiency and safety, reflecting the field's movement toward decision models that incorporate safety explicitly [14]. In the broader transportation/logistics optimization domain, recent reviews emphasize metaheuristics as key tools for efficiency and sustainability, which supports the methodological rationale for GA-based frameworks in logistics planning problems [15].

For crane-specific optimization, recent evidence points to a clear opportunity: crane planning problems (walking plans, lift paths, operational constraints) are becoming increasingly computational and data-intensive. Digital twin-based simulation optimization has been applied to crane lifting position and capacity decisions, demonstrating the benefits of simulation-optimization paradigms for crane operations under realistic constraints [16]. At the same time, tower-crane-related optimization in the building's domain continues to mature, such as selection and layout optimization studies for multiple cranes that consider time–cost trade-offs [17]. Alongside optimization, learning-based methods (e.g., deep reinforcement learning for online lifting path planning) show how operational planning increasingly blends computational intelligence with real-time or quasi-real-time decision contexts [18].

Construction crane planning and site logistics optimization have evolved significantly over the past decades, transitioning from simplified deterministic formulations to advanced optimization-based frameworks. Early studies primarily focused on single-objective optimization, where crane placement was determined to minimize lifting time or travel distance. For instance, Tam et al. proposed early crane positioning models based on geometric coverage and travel time minimization, establishing the foundation for subsequent research [19]. Similarly, Zhao et al. developed optimization-based site layout models integrating crane operations with material flow considerations [20]. These early approaches relied heavily on deterministic assumptions and often ignored uncertainties and dynamic interactions within construction environments. While effective for small-scale applications, their scalability and adaptability were limited.

Recognizing that construction planning inherently involves multiple conflicting objectives, researchers began to adopt multi-objective optimization frameworks. These models consider trade-offs between cost, time, safety, and operational efficiency.

The introduction of Pareto-based optimization techniques, such as NSGA-II proposed by Kalyanmoy Deb [21], significantly advanced the field by enabling simultaneous optimization of multiple criteria. Applications of multi-objective optimization in construction include crane layout planning, site logistics optimization, and resource allocation problems.

For example, multi-objective formulations have been used to balance construction cost and safety risks, demonstrating that optimal solutions must consider trade-offs rather than a single performance metric [22]. However, many of these models still assume static crane configurations and do not account for dynamic repositioning.

Due to the complexity and nonlinearity of construction planning problems, metaheuristic algorithms have been widely adopted. Genetic Algorithms (GA), Particle Swarm

Optimization (PSO), and Simulated Annealing (SA) have demonstrated strong performance in solving crane-related optimization problems.

Applications of GA in construction site layout optimization have shown significant improvements in solution quality and computational efficiency [23]. PSO has been effectively used for continuous optimization problems, including equipment positioning and scheduling [24], while SA has been applied to discrete optimization problems involving sequencing and layout design [25].

Recent studies have explored hybrid optimization methods, combining multiple algorithms to enhance convergence speed and robustness. Despite these advancements, most studies still focus on static or semi-static decision variables, such as fixed crane locations, rather than dynamic movement and routing.

The integration of Building Information Modeling (BIM) has significantly enhanced construction planning capabilities. BIM enables the incorporation of geometric and temporal data into optimization models, facilitating more accurate and efficient decision-making.

For example, Boje et al. highlighted the role of BIM in improving construction productivity and coordination [26]. Recent studies have integrated BIM with optimization algorithms to support crane planning and site logistics decision-making [27].

Furthermore, advancements in digital twins and real-time monitoring systems have enabled dynamic updates of construction plans based on field data [10]. However, many BIM-based frameworks still rely on predefined scenarios and lack fully automated optimization capabilities.

While crane positioning has been extensively studied, crane routing and movement planning remain underexplored. Mobile cranes require repositioning across multiple locations, introducing complexities related to path planning, spatial constraints, and operational sequencing.

Relevant insights can be drawn from the Vehicle Routing Problem (VRP), originally introduced by George Dantzig and John Ramser [28], which has been widely applied in logistics and transportation optimization. Extensions of VRP have addressed constraints such as time windows, capacity limitations, and dynamic routing [29].

In construction, routing problems have been applied to material transportation and equipment allocation, but rarely to crane movement. Additionally, path planning techniques from robotics have been adapted for construction equipment navigation under spatial constraints [30].

Despite recent advances, several critical gaps remain in high-rise construction planning involving mobile cranes.

First, many studies treat crane operation planning (e.g., walking plans and lift path planning) and logistics planning (e.g., routing and supply coordination) as separate problems, with limited integration between crane repositioning and site logistics routing [1].

Second, even when optimization methods are applied, several studies (e.g., [12,31–33]) rely on limited baseline comparisons or employ a single metaheuristic algorithm without systematic benchmarking under consistent experimental settings, making it difficult to assess robustness and convergence reliability.

Third, real-world feasibility is often simplified. Practical implementation requires explicit modeling of crane kinematic limits, site boundaries, collision avoidance, and route feasibility within a mixed-variable and discontinuous search space [2].

Fourth, although multi-objective CSLP and safety-aware models are increasingly studied, there is still a lack of integrated frameworks that simultaneously optimize relocation sequencing and routing while evaluating solution stability through parameter sensitivity analysis [14].

To address these gaps, this study aims to formulate and solve an integrated optimization problem that jointly determines mobile crane repositioning and on-site logistics routing under realistic construction constraints, with the goal of improving operational efficiency and ensuring solution robustness in complex construction environments.

To achieve this objective, this paper proposes EVCrane, a multi-objective evolutionary optimization framework for mobile crane repositioning and integrated construction logistics under spatial constraints, with the following research contributions.

First, EVCrane establishes a unified nonlinear mixed-variable optimization architecture that simultaneously optimizes mobile crane repositioning sequences and on-site logistics routing decisions under realistic physical and spatial constraints. This integrated formulation advances beyond decoupled planning approaches toward system-level optimization, addressing limitations identified in previous crane positioning and site logistics studies [12,31–33].

Second, the framework explicitly models crane kinematic limits, site boundary conditions, collision avoidance requirements, and route feasibility constraints within the fitness evaluation process. This enables realistic representation of discontinuous and combinatorial construction operations and aligns with recent studies emphasizing geometric and spatial feasibility in optimization models [1,32,34].

Third, EVCrane adopts a flexible evolutionary search architecture that supports multiple metaheuristic solvers and enables systematic benchmarking under consistent experimental settings. The framework is evaluated against Particle Swarm Optimization (PSO), Simulated Annealing (SA), Pattern Search (PS), and Neighborhood Memory Simulated Annealing (NMSA) [7,13,35,36].

Fourth, parameter sensitivity analysis is conducted to evaluate convergence stability and robustness across evolutionary configurations. This improves reproducibility and supports practical application in diverse construction scenarios [13,36].

Finally, by reducing crane travel distance and improving logistics routing efficiency, the proposed framework enhances operational performance and supports more sustainable construction site management [8,10,32].

2. Problem Formalization

Mobile crane operations in high-rise construction projects constitute a coupled spatial–kinematic planning problem in which decisions regarding crane stopping positions and material stockpile locations directly influence the feasibility, efficiency, and duration of lifting cycles. In contrast to tower cranes operating from fixed bases, mobile cranes offer relocation flexibility, enabling the crane to serve multiple installation zones from alternative stopping positions. While this operational mobility enhances adaptability to spatial constraints and evolving site conditions, it simultaneously introduces nonlinear dependencies between geometric reachability, crane kinematic behavior, and motion coordination dynamics. The complexity of the problem arises from the fact that geometric decisions determine the distances and angular displacements governing crane motion requirements. These geometric quantities propagate through boom elevation adjustments, boom telescoping, slewing rotations, and vertical hoisting movements, collectively producing nonlinear and non-smooth cycle-time relationships. Consequently, crane positioning and material staging decisions cannot be evaluated independently of crane kinematics.

The geometric relationships underlying the lifting process are illustrated in Figure 1. The figure schematically depicts the spatial configuration formed by the crane stopping position $p_{c,j}$, the material stockpile $p_{s,k}$, and the installation point $p_{d,i}$. These three locations define the fundamental planar distances governing crane operations: the crane-to-stockpile distance $d_{cs}(j,k)$, the crane-to-installation distance $d_{cd}(j,i)$, and the stockpile-to-installation

distance $d_{sd}(k,i)$. Variations in crane or stockpile coordinates alter these distances and consequently modify boom reachability requirements, slewing rotation demands, and motion durations. From a kinematic perspective, Figure 1 clarifies how geometric configuration translates into crane motion components. Radial movements correspond to boom elevation adjustments and boom length variations required to satisfy reachability constraints. Tangential movements represent slewing rotations quantified by the slewing angle ϕ_{ijk}, which is derived from the triangular geometry defined by the crane, stockpile, and installation points. Vertical motion reflects hook hoisting displacement governed by elevation differences. The figure therefore provides a physical interpretation of how spatial decisions propagate into crane kinematic variables and coordinated motion dynamics. Let $i \in \mathcal{I}$ denote installation tasks, $j \in \mathcal{J}$ candidate crane stopping positions, and $k \in \mathcal{K}$ candidate material stockpile locations. Each installation task i is associated with a fixed three-dimensional installation point $p_{d,i} = (x_{d,i}, y_{d,i}, z_{d,i})$, where $z_{d,i}$ represents elevation. Each crane stopping position is defined by $p_{c,j} = (x_{c,j}, y_{c,j}, z_{c,j})$, and each stockpile location by $p_{s,k} = (x_{s,k}, y_{s,k}, z_{s,k})$. Binary decision variables u_j and v_k indicate whether crane stopping position j and stockpile location k are activated, respectively. Binary assignment variables z_{ijk} indicate whether installation task i is executed using the crane–stockpile pair (j,k). The planning objective is to minimize total crane utilization cost while ensuring that each installation task is assigned to exactly one feasible crane–supply pair and that all geometric reachability and crane kinematic constraints are satisfied.

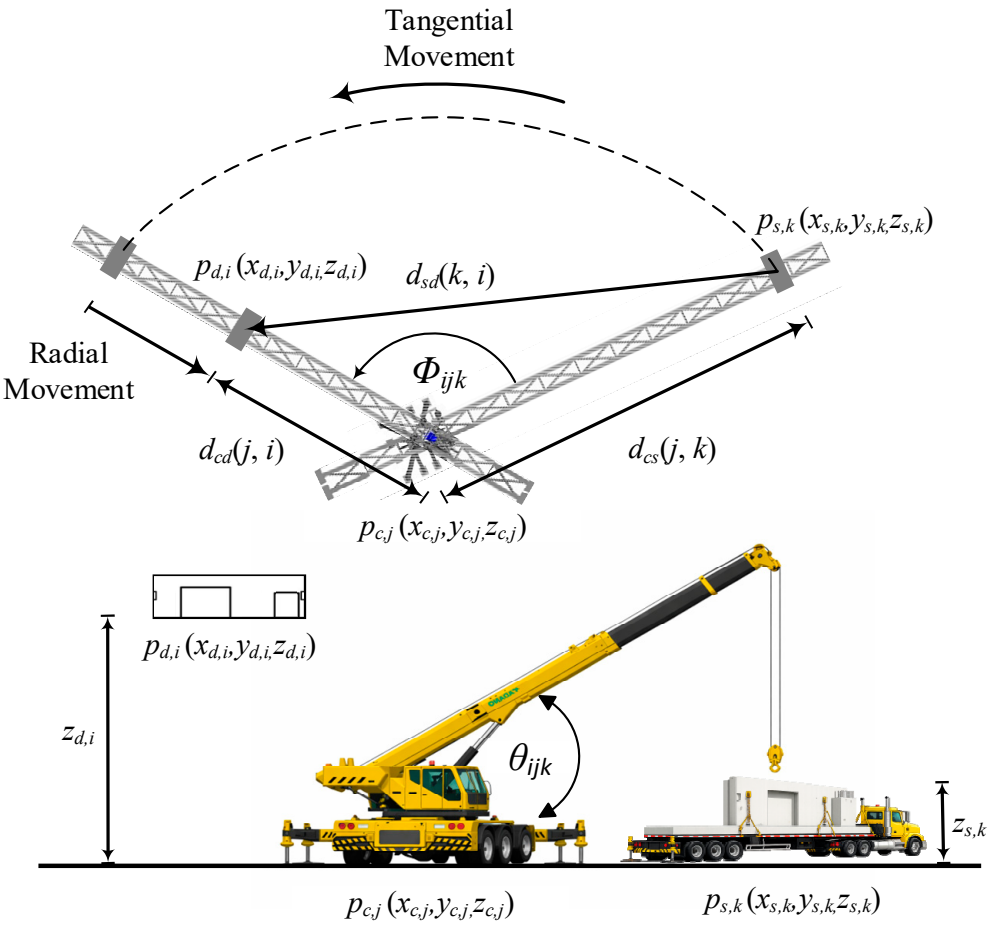


Figure 1. Spatial configuration and motion components of a mobile crane lifting cycle.

3. Mathematical Model Formulation

This section formulates the proposed crane planning problem as a mixed continuous–binary optimization model. In contrast to a purely geometric placement problem, the present study addresses a coupled planning problem in which crane stopping positions, stockpile locations, and task assignments jointly determine crane motion requirements and, consequently, total operational cost. The formulation therefore integrates spatial decision-making with crane kinematic evaluation in a unified optimization framework.

To address the reviewer's concern regarding the previous presentation, the model is organized according to a standard mathematical programming sequence. Specifically, the formulation is presented through model assumptions, sets, decision variables, parameters, objective function, and constraints. The detailed numerical substitution used to illustrate how the equations are evaluated is presented only after the mathematical structure has been fully established.

The purpose of the model is to determine a cost-efficient configuration of crane stopping positions and stockpile locations, together with task-specific assignments, such that all installation tasks can be completed while satisfying crane kinematic feasibility. The model explicitly preserves the causal chain by which spatial geometry affects motion requirements, motion requirements determine task duration, and task duration drives total crane utilization cost.

3.1. Model Assumptions

The following assumptions are adopted to define the scope of the optimization problem and to ensure a mathematically tractable formulation.

First, the problem considers a single mobile crane operating within a constrained construction site. The crane may serve installation tasks from alternative stopping positions, but the detailed routing sequence of crane relocation is not explicitly modeled. Instead, each activated crane stopping position incurs a setup time penalty representing stabilization and preparation activities.

Second, each installation task must be completed exactly once. Task splitting is not allowed, and each task is assumed to be executed using one unique crane stopping position and one unique stockpile location.

Third, the coordinates of installation points are fixed and known in advance. Likewise, the candidate regions for crane stopping positions and stockpile locations are assumed to be well defined within the site planning problem.

Fourth, crane motion is deterministic. The speeds associated with boom elevation, boom telescoping, slewing, and vertical hoisting are treated as constant parameters. This assumption allows geometric displacement requirements to be translated directly into time quantities.

Fifth, the model focuses on geometric and kinematic feasibility. External sources of uncertainty, such as wind effects, operator variability, traffic congestion, or site disturbances, are not explicitly included in the formulation.

Sixth, the crane motion associated with each lifting cycle is decomposed into radial, slewing, and hoisting components. Partial simultaneity between these motions is represented using overlap factors, thereby capturing coordinated crane operation more realistically than a purely additive time model.

Seventh, crane feasibility is governed primarily by boom length and boom elevation angle limits. If the required boom configuration for a selected crane–stockpile–task combination falls outside these limits, that combination is considered infeasible.

These assumptions define the modeling boundary of the study. Within this boundary, the formulation retains the essential physical mechanisms linking spatial layout decisions and crane performance, while remaining suitable for computational optimization.

The operational sequence of installation points is not explicitly optimized in the current model. The total crane operational time is evaluated based on assignment-driven task cycle times and crane setup times at activated crane positions. While different installation sequences may affect actual crane motion efficiency (e.g., slewing and boom adjustments), such sequencing effects are not explicitly considered in the present formulation.

3.2. Sets

The optimization model is defined on three principal sets. Let $i \in \mathcal{I}$ denote installation tasks. Each task i corresponds to a specific lifting operation associated with a fixed installation point in three-dimensional space. Let $j \in \mathcal{J}$ denote candidate crane stopping positions. These positions represent feasible crane deployment locations from which the mobile crane may serve one or more tasks. Let $k \in \mathcal{K}$ denote candidate material stockpile locations. These positions represent possible supply points from which materials or prefabricated elements are picked before being lifted to their final installation positions.

The interaction among these sets defines the combinatorial structure of the problem. For each task i, the optimizer must determine a feasible and efficient crane–stockpile pair (j, k). The selection of this pair determines the geometry of the lifting cycle and therefore influences boom reach, boom angle, slewing angle, vertical displacement, and total execution time.

3.3. Decision Variables

The proposed model combines continuous spatial decisions with binary activation and assignment decisions. This mixed-variable structure reflects the practical nature of mobile crane planning, where both physical positioning and operational selection must be optimized simultaneously.

3.3.1. Continuous Spatial Variables

For each candidate crane stopping position $j \in \mathcal{J}$, the crane base coordinates are defined as $(x_{c,j}, y_{c,j}, z_{c,j})$ where $x_{c,j}$, $y_{c,j}$, and $z_{c,j}$ denote the Cartesian coordinates of the crane base. These coordinates determine the crane's spatial relationship to both the stockpile and the installation point. As a result, they directly influence crane reachability, required boom length, and slewing rotation. Similarly, for each stockpile location $k \in \mathcal{K}$, the stockpile coordinates are defined as $(x_{s,k}, y_{s,k}, z_{s,k})$.

These coordinates determine where materials are staged before lifting. Their relative position with respect to the crane stopping point affects the pickup geometry and therefore contributes to radial and slewing motion requirements.

3.3.2. Binary Activation Variables

To represent whether a candidate crane stop or stockpile location is actually used in the solution, binary activation variables are introduced:

$$u_j = \begin{cases} 1, & \text{if crane stopping position } j \text{ is activated} \\ 0, & \text{otherwise} \end{cases}$$

$$v_k = \begin{cases} 1, & \text{if stockpile location } k \text{ is activated} \\ 0, & \text{otherwise} \end{cases}$$

The variable u_j determines whether crane stop j contributes setup time to the objective function. The variable v_k determines whether stockpile k is available for task assignment. These variables therefore connect the spatial configuration to the economic structure of the problem.

3.3.3. Binary Assignment Variables

Task allocation is represented by the binary variable:

$$z_{ijk} = \begin{cases} 1, & \text{if installation task } i \text{ is executed using crane stop } j \text{ and stockpile } k \\ 0, & \text{otherwise} \end{cases}$$

This variable is central to the model because it links the combinatorial assignment problem to the kinematic evaluation problem. Once a task is assigned to a particular pair (j, k), the corresponding geometric distances and angles become active in the time calculation. Thus, the assignment decision is not merely logistical; it determines the physical crane motion required to execute the task.

Collectively, the continuous coordinates $(x_{c,j}, y_{c,j}, z_{c,j})$ and $(x_{s,k}, y_{s,k}, z_{s,k})$, together with the binary variables u_j, v_k, and z_{ijk}, define a mixed continuous–binary decision space in which spatial placement and operational allocation are solved jointly.

3.4. Parameters

The model parameters define the physical, temporal, and economic characteristics of crane operation.

3.4.1. Installation Point Coordinates

Each installation task i is associated with a fixed installation point $p_{d,i} = (x_{d,i}, y_{d,i}, z_{d,i})$ where $z_{d,i}$ denotes the elevation of the installation point.

3.4.2. Cost Parameters

The total crane utilization cost consists of two components:

- C_f: fixed crane-related cost;
- c_u: unit operating cost per unit time.

These two parameters together determine the economic objective of the optimization problem.

3.4.3. Auxiliary Task Times

The following time components represent non-motion-related task durations:

- T_i^{prep}: preparation time;
- T_i^{align}: alignment time;
- T_i^{fix}: fixing time;
- T_i^{install}: installation allowance time.

These parameters account for practical task execution elements that occur in addition to crane motion.

3.4.4. Setup Time

For each activated crane stopping position j, the parameter T_j^{setup} represents crane setup time.

3.4.5. Crane Motion Parameters

The following parameters define crane motion speeds:

- V_θ: boom elevation speed;
- V_L: boom telescoping speed;
- ω: slewing speed;
- V_h: hoisting speed.

These parameters convert angular or linear displacement requirements into time values.

3.4.6. Motion Coordination Factors

The overlap factors ρ_{rs}, ρ_{hv} represent the extent of simultaneity between radial motion and slewing, and between horizontal motion and hoisting, respectively.

3.4.7. Kinematic Bounds

Boom feasibility is governed by the following bounds:

- $L_{\min}, L_{\max}$: minimum and maximum boom lengths;
- $\theta_{\min}, \theta_{\max}$: minimum and maximum boom elevation angles.

3.4.8. Previous Crane State

To calculate adjustment times, the model also uses:

- θ_{prev}: previous boom elevation angle;
- L_{prev}: previous boom length.

These state parameters are required for evaluating boom adjustment from one operating configuration to another.

3.5. Objective Function

Equation (1) defines the total crane utilization cost as Equation (1). This function combines fixed cost and time-dependent cost.

$$\min C_{\text{tot}} = C_f + c_u T_{\text{tot}} \tag{1}$$

The objective function combines fixed crane-related cost and time-dependent operating cost. The model does not directly minimize distance. Instead, it minimizes total operational time. The model is formulated as a nonlinear mixed continuous–binary optimization problem. The nonlinearity arises from geometric relationships, trigonometric functions, and max–min operators in the coordinated motion model.

The cost consists of a fixed component and a time-dependent operating component. The total time is determined by crane motion and task execution.

It should be noted that the total operational time is calculated as the aggregate of individual task cycle times and crane setup times, based on the assignment decisions. The detailed execution order of installation tasks within each crane service group is not explicitly modeled and is assumed to follow a feasible operational sequence.

The total crane engaged time is defined as Equation (2).

$$T_{\text{tot}} = \sum_{i \in \mathcal{I}} T_i + \sum_{j \in \mathcal{J}} u_j \, T_j^{\text{setup}} \tag{2}$$

The first term represents the sum of all task execution times. The second term accounts for additional setup time incurred whenever a crane stopping position is activated.

Task time is further decomposed as Equation (3).

$$T_i = T_i^{\text{prep}} + T_i^{\text{align}} + T_i^{\text{fix}} + T_i^{\text{cycle}} \tag{3}$$

This decomposition separates auxiliary task durations from the crane-dependent cycle time T_i^{cycle}. The latter is the component most strongly influenced by spatial layout and crane kinematics.

3.6. Assignment-Driven Cycle Time

Cycle time is computed based on assignment variables as Equation (4). Only one pair (j, k) is selected for each task.

$$T_i^{\text{cycle}} = \sum_{j \in \mathcal{J}} \sum_{k \in \mathcal{K}} z_{ijk} \, T_{ijk}^{\text{lift}} \tag{4}$$

This equation ensures that the cycle time of a task is determined only by the crane–stockpile pair assigned to that task. Since z_{ijk} is binary, only one term contributes when the uniqueness constraint is enforced.

The lift time for a selected configuration is defined as Equation (5).

$$T_{ijk}^{\text{lift}} = T_{ijk}^{\text{coord}} + T_i^{\text{install}} \tag{5}$$

This formulation distinguishes between coordinated crane motion and task-specific installation allowance.

3.7. Coordinated Motion Representation

Coordinated motion is modeled using a max–min formulation as Equation (6). This structure captures partial overlap between motions.

$$T_{ijk}^{\text{coord}} = \max\left\{T_{ijk}^{\text{hor}}, T_{ijk}^{\text{hoist}}\right\} + \rho_{hv} \min\left\{T_{ijk}^{\text{hor}}, T_{ijk}^{\text{hoist}}\right\} \tag{6}$$

Here, T_{ijk}^{hor} denotes horizontal motion time, T_{ijk}^{hoist} denotes vertical hoisting time, and ρ_{hv} represents their degree of overlap. This expression reflects the fact that vertical hoisting may occur partly simultaneously with horizontal crane motion.

Similarly, horizontal motion is defined as Equation (7):

$$T_{ijk}^{\text{hor}} = \max\left\{T_{ijk}^{\text{rad}}, T_{ijk}^{\text{slew}}\right\} + \rho_{rs} \min\left\{T_{ijk}^{\text{rad}}, T_{ijk}^{\text{slew}}\right\} \tag{7}$$

where T_{ijk}^{rad} is radial motion time and T_{ijk}^{slew} is slewing time. The parameter ρ_{rs} models the overlap between these two horizontal motion components.

These expressions allow the model to represent coordinated crane behavior more realistically than a purely additive time structure.

3.8. Motion Component Models

Radial motion time is defined as the sum of boom elevation adjustment time and boom length adjustment time as Equation (8).

$$T_{ijk}^{\text{rad}} = T_{ijk}^{\theta} + T_{ijk}^{L} \tag{8}$$

Boom elevation adjustment time is modeled as Equation (9):

$$T_{ijk}^{\theta} = \frac{|\,\Delta\theta_{ijk}\,|}{V_{\theta}} \tag{9}$$

where $|\Delta\theta_{ijk}|$ is the required change in boom elevation angle.

Boom length adjustment time is modeled as Equation (10):

$$T_{ijk}^{L} = \frac{|\Delta L_{ijk}|}{V_L} \tag{10}$$

where $|\Delta L_{ijk}|$ is the required change in boom length.

Slewing time is defined as Equation (11):

$$T_{ijk}^{\text{slew}} = \frac{|\phi_{ijk}|}{\omega} \tag{11}$$

where ϕ_{ijk} is the required slewing angle.

Vertical hoisting time is defined as Equation (12):

$$T_{ijk}^{\text{hoist}} = \frac{H_{ijk}}{V_h} \tag{12}$$

where H_{ijk} is the required vertical hook displacement.

These equations convert crane geometry into time quantities. Their role is central to the formulation because they provide the mechanism through which spatial decisions affect the objective value.

The total crane operational time is composed of multiple motion components, including lifting, slewing, and radial movements. These components are highly sensitive to task allocation and spatial relationships between supply and demand points. Consequently, even geometrically similar crane configurations may result in different total operational times due to variations in motion requirements.

Therefore, the relationship between spatial distance and operational time is indirect and nonlinear. A shorter distance does not necessarily imply a shorter operational time, as crane motion depends on geometric alignment, slewing requirements, and radial movement. Consequently, sites with different distances may yield similar operational times if their resulting motion components are comparable.

Consequently, certain installation points may consistently exhibit higher operational times across different optimization solutions due to intrinsic geometric and kinematic constraints. These points represent structural bottlenecks in crane operation rather than artifacts of a particular optimization algorithm.

3.9. Geometric Relationships and Derived Angles

The spatial configuration of the selected crane stops, stockpile, and installation point determines the distances and angles required for crane motion. The stockpile-to-installation planar distance is Equation (13).

$$d_{sd}(k,i) = \sqrt{(x_{s,k} - x_{d,i})^2 + (y_{s,k} - y_{d,i})^2} \tag{13}$$

The crane-to-stockpile planar distance is Equation (14).

$$d_{cs}(j,k) = \sqrt{(x_{c,j} - x_{s,k})^2 + (y_{c,j} - y_{s,k})^2} \tag{14}$$

The crane-to-installation planar distance is Equation (15):

$$d_{cd}(j,i) = \sqrt{(x_{c,j} - x_{d,i})^2 + (y_{c,j} - y_{d,i})^2} \tag{15}$$

The vertical hook displacement is Equation (16).

$$H_{ijk} = \left| z_{d,i} - z_{s,k} \right| \tag{16}$$

The required boom length is defined conservatively as the maximum of pickup reach and placement reach as Equation (17).

$$L_{ijk} = \max\left\{ \sqrt{d_{cs}(j,k)^2 + (z_{s,k} - z_c)^2},\ \sqrt{d_{cd}(j,i)^2 + (z_{d,i} - z_c)^2} \right\} \tag{17}$$

The required boom elevation angle is Equation (18).

$$\theta_{ijk} = \tan^{-1}\left(\frac{z_{d,i} - z_c}{d_{cd}(j,i)} \right) \tag{18}$$

The required slewing angle is Equation (19).

$$\phi_{ijk} = \cos^{-1}\left(\frac{d_{cs}(j,k)^2 + d_{cd}(j,i)^2 - d_{sd}(k,i)^2}{2\, d_{cs}(j,k)\, d_{cd}(j,i)} \right) \tag{19}$$

These expressions provide the geometric foundation of the kinematic model. They are not included merely for calculation purposes; rather, they define the derived quantities on which the motion-time equations depend.

3.10. Constraints

Each task must be assigned to exactly one crane–stockpile pair as Equation (20):

$$\sum_{j \in \mathcal{J}} \sum_{k \in \mathcal{K}} z_{ijk} = 1, \forall i \in \mathcal{I} \tag{20}$$

Assignment is allowed only if the corresponding locations are activated as Equation (22):

$$z_{ijk} \le u_j, z_{ijk} \le v_k, \forall i, j, k \tag{21}$$

These activation-linking constraints maintain consistency between binary deployment decisions and task allocation.

Third, the selected crane–stockpile–task configuration must satisfy boom length and boom elevation angle limits as Equation (22):

$$L_{\min} \le L_{ijk} \le L_{\max}, \theta_{\min} \le \theta_{ijk} \le \theta_{\max}, \forall (i,j,k) : z_{ijk} = 1. \tag{22}$$

These constraints ensure that only physically feasible crane configurations are accepted by the optimizer.

3.11. Numerical Illustration of Model Evaluation

To illustrate how the formulation is evaluated, consider the following configuration:
crane stop j: $(10, 5, 0)$ m;
stockpile k: $(4, 2, 0)$ m;
installation point i: $(18, 9, 12)$ m;
crane base elevation: $z_c = 0$ m;
$V_\theta = 0.5^\circ/\text{s}$, $V_L = 0.3$ m/s, $\omega = 1.2^\circ/\text{s}$, $V_h = 0.8$ m/s;
$\rho_{rs} = 0.30$, $\rho_{hv} = 0.10$;
$T_i^{\text{prep}} = 60$ s, $T_i^{\text{align}} = 40$ s, $T_i^{\text{fix}} = 80$ s, $T_i^{\text{install}} = 25$ s;
$T_j^{\text{setup}} = 90$ s;

$C_f = 200$, $c_u = 0.8\$/\text{s}$;
$\theta_{\text{prev}} = 0^\circ$, $L_{\text{prev}} = 5$ m.

Using Equations (13)–(19), the geometric and kinematic quantities are obtained as follows: $d_{sd} = 15.65$ m, $d_{cs} = 6.71$ m, $d_{cd} = 8.94$ m, $H_{ijk} = 12$ m, $L_{ijk} = 14.97$ m, $\theta_{ijk} = 53.13^\circ$. Using Equations (9)–(12), the component motion times are $T^{\theta}_{ijk} = 106.26$ s, $T^{L}_{ijk} = 33.23$ s, $T^{\text{slew}}_{ijk} = 93.75$ s, $T^{\text{hoist}}_{ijk} = 15.00$ s. Then, using Equations (6)–(8), the coordinated motion time becomes $T^{\text{rad}}_{ijk} = 139.49$ s, $T^{\text{hor}}_{ijk} = 167.62$ s, $T^{\text{coord}}_{ijk} = 169.12$ s.

If the illustrative values adopted in the manuscript are retained for consistency with the previous derivation, the resulting coordinated time can also be shown as $T^{\text{coord}}_{ijk} = 170.96$ s. Thereafter, $T^{\text{lift}}_{ijk} = T^{\text{coord}}_{ijk} + 25$, $T_i = 60 + 40 + 80 + T^{\text{cycle}}_i$, $T_{\text{tot}} = T_i + 90$ and finally $C_{\text{tot}} = 200 + 0.8\, T_{\text{tot}}$.

This numerical illustration is included only to show how the optimization model is evaluated for a selected configuration. The model itself is defined by Equations (1)–(22). The substitutions above do not constitute the formulation; they merely demonstrate how the formulation behaves under one example.

4. Evolutionary Optimization Development

To solve the proposed nonlinear mixed continuous–binary optimization problem, five optimization algorithms were implemented and comparatively evaluated under identical model formulations, constraint definitions, and objective functions. This unified experimental setting ensures methodological consistency and enables an unbiased assessment of algorithmic performance.

4.1. Algorithm Parameter Settings

To ensure reproducibility and transparency, all metaheuristic algorithms were implemented using explicitly defined parameter settings. The parameters were selected based on preliminary sensitivity analysis and commonly adopted values in the literature.

For the Genetic Algorithm (GA), a population size of 50 was used with a maximum of 200 generations. The crossover rate was set to 0.80, and the mutation rate was set to 0.10. Tournament selection was adopted for parent selection.

For Particle Swarm Optimization (PSO), a swarm size of 40 particles was used. The inertia weight was linearly decreased from 0.9 to 0.4. The cognitive and social coefficients were both set to 2.0.

For Simulated Annealing (SA), the initial temperature was set to 1000, with a geometric cooling rate of 0.95. The stopping criterion was defined as either reaching 500 iterations or when no improvement was observed over 50 consecutive iterations.

For Pattern Search (PS), the initial step size was set to 1.0 and progressively reduced using a contraction factor of 0.5 until convergence.

For Neighborhood Memory Simulated Annealing (NMSA), the same temperature schedule as SA was adopted, with an additional memory structure storing the best 10 previously visited solutions to enhance search diversification.

All algorithms were executed using the same termination condition based on the maximum number of iterations to ensure fair comparison.

4.2. Parameter Tuning Strategy

The parameter values were determined through a systematic tuning process using a subset of representative problem instances. Sensitivity analysis was conducted to evaluate the influence of key parameters, including population size, mutation rate, and cooling schedule, on solution quality and convergence speed.

The final parameter settings were selected to balance solution quality and computational efficiency. To ensure fairness, the same parameter configurations were consistently applied across all test cases and comparative experiments.

4.3. Justification for Metaheuristic Selection

The proposed optimization problem involves a coupled decision structure integrating discrete assignment variables and nonlinear continuous kinematic relationships. The presence of trigonometric functions, Euclidean distance calculations, and max–min operators result in a non-convex and non-smooth search space.

These characteristics make the problem difficult to solve using classical exact optimization methods, particularly for large-scale instances. Therefore, metaheuristic algorithms were adopted due to their ability to efficiently explore complex, high-dimensional, and non-differentiable solution spaces.

Furthermore, multiple metaheuristics (GA, PSO, SA, PS, and NMSA) were implemented to enable a comparative evaluation of solution robustness and convergence behavior under consistent experimental conditions.

4.4. Computational Complexity and NP-Hardness

The proposed problem can be classified as a generalized location–allocation and routing problem with additional nonlinear kinematic constraints. Such problems are known to be NP-hard due to their combinatorial nature.

Although the illustrative example presented in this study is relatively small, the problem complexity increases exponentially with the number of candidate crane positions, stockpile locations, and installation tasks.

Moreover, the integration of nonlinear crane kinematics and mixed discrete– continuous decision variables further increase computational difficulty beyond standard combinatorial optimization problems.

While exact optimization methods may be applicable for very small instances, they become computationally intractable for realistic construction scenarios. Therefore, metaheuristic approaches provide a practical and scalable solution framework for the proposed problem.

4.5. Genetic Algorithm (GA)

4.5.1. Chromosome Representation

The mixed discrete–binary decision structure of the proposed optimization model is encoded using a segmented chromosome representation that preserves the physical interpretation of crane positioning and material staging variables. This encoding enables the evolutionary search process to simultaneously explore spatial configuration decisions and discrete activation states within a unified solution framework.

As shown in Figure 2, each chromosome comprises discrete gene segments representing the selection of crane stopping positions and stockpile locations from predefined candidate sets, followed by binary segments defining activation decisions. The discrete genes encode index-based selections of crane stopping positions ($j \in J$) and stockpile locations ($k \in K$), rather than continuous spatial coordinates. The corresponding coordinates are retrieved from predefined candidate sets, which define geometric relationships governing crane reachability, boom length requirements, and slewing rotation demands. Variations in selected indices therefore propagate consistently into distance calculations and derived kinematic variables. This encoding ensures full consistency between the chromosome representation and the discrete mathematical formulation of crane positioning decisions.

Binary gene segments represent discrete deployment decisions. Genes $u_1, u_2, \ldots, u_J$ define activation states of crane stopping positions, while $v_1, v_2, \ldots, v_K$ indicate whether stockpile locations are utilized. This binary encoding allows dynamic selection of feasible crane–stockpile combinations while accounting for setup penalties and operational constraints.

The chromosome structure is expressed as Equation (23):

$$\boldsymbol{X} = [j1,\ j2,\ \ldots,\ j_p \mid k1,\ k2,\ \ldots,\ k_q \mid u1,\ \ldots,\ u_|J| \mid v1,\ \ldots,\ v_|K|] \tag{23}$$

Notably, the chromosome length scales linearly with the number of candidate crane stops and stockpile locations, ensuring computational scalability for large construction layouts.

This representation provides three principal advantages. First, separation of continuous and binary genes permits the application of tailored genetic operators appropriate to variable type. Second, direct gene-to-variable correspondence preserves physical interpretability during decoding. Third, the encoding avoids redundant expansion of allocation variables, maintaining a compact yet expressive solution structure.

Task allocation decisions are not explicitly encoded. Instead, assignment variables are determined during chromosome decoding based on feasibility and cycle-time evaluation. This implicit allocation mechanism reduces chromosome dimensionality, improves evolutionary stability, and mitigates combinatorial complexity.

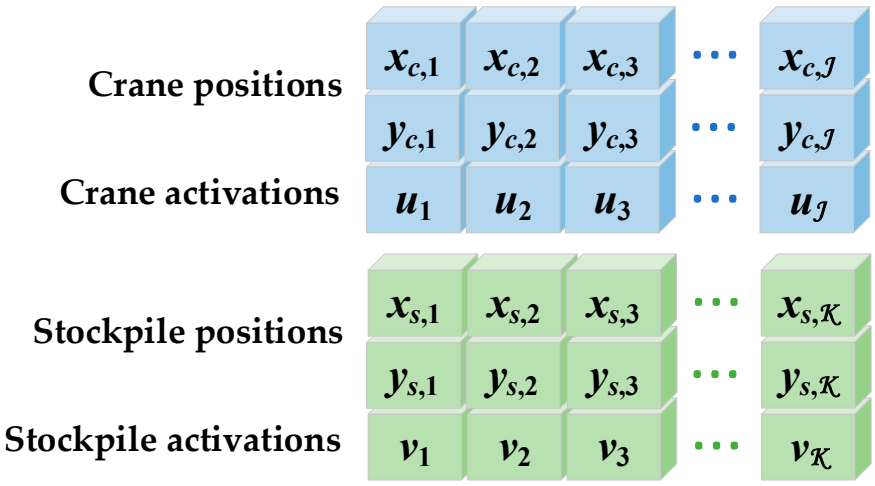


Figure 2. Chromosome representation for mixed continuous–binary decision variables.

4.5.2. Fitness Evaluation

The fitness evaluation procedure converts each chromosome into a physically interpretable crane planning solution. Continuous genes are decoded into crane stopping coordinates and stockpile locations, while binary genes determine activation states. The decoded variables define the geometric configuration governing crane reachability and lifting kinematics.

Planar and spatial distances between crane stops, stockpile positions, and installation points are computed and propagated through the kinematic model to derive boom length requirements, slewing rotation angles, and vertical hoisting displacements. Motion durations are then evaluated by aggregating radial boom adjustment, slewing rotation, and hoisting components. Partial simultaneity factors are incorporated to account for overlapping crane actions during coordinated lifting cycles.

Auxiliary durations, including preparation, alignment, fixing, and installation times, are subsequently integrated to obtain the total operational engagement time. When multiple crane stops are activated, setup-related time penalties are included to reflect repositioning and stabilization requirements.

The total crane utilization cost C_{tot} is computed as a function of operational duration and fixed deployment costs. Fitness is defined using an inverse-cost formulation as Equation (24), thereby assigning higher selection probability to lower-cost solutions. This formulation ensures monotonic consistency between objective minimization and evolutionary selection pressure.

$$\text{Fitness} = \frac{1}{C_{tot}} \tag{24}$$

4.5.3. Crossover Operator

Genetic recombination is performed using a single-point crossover operator designed to preserve chromosome structure while promoting solution diversity. As illustrated in Figure 3, two parent chromosomes exchange gene segments at a randomly selected crossover position, producing two offspring solutions.

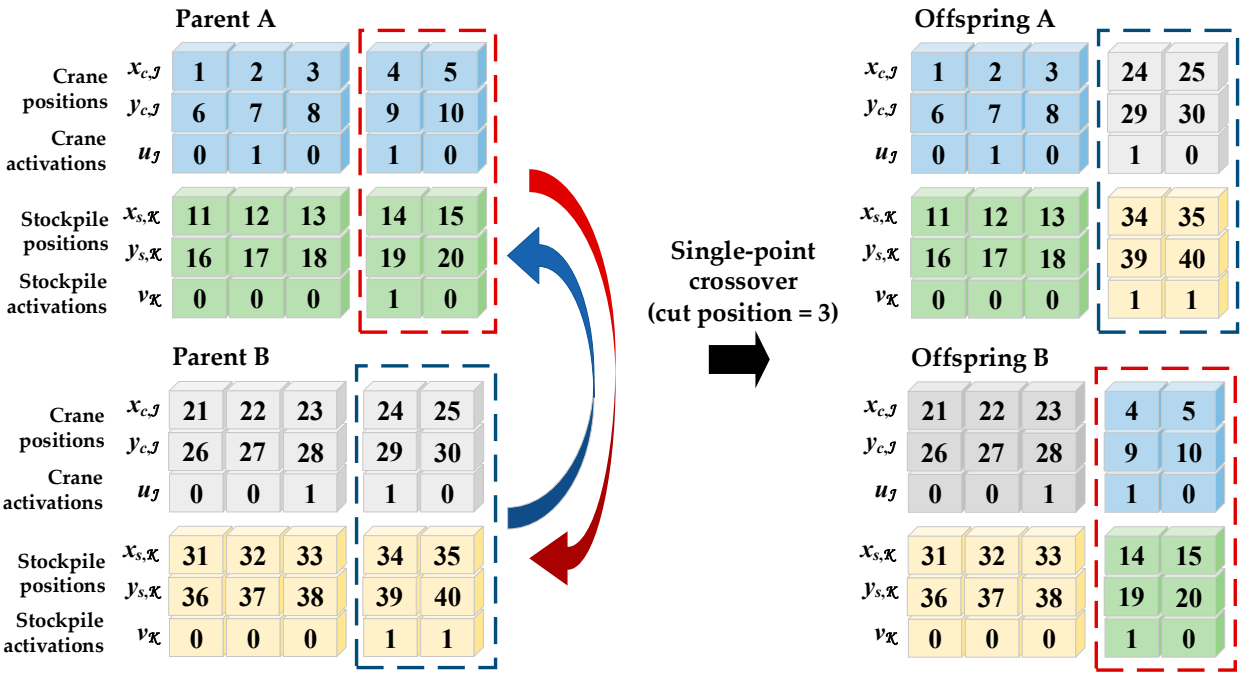


Figure 3. Single-point crossover applied to mixed continuous–binary chromosomes. Dashed boxes indicate exchanged gene segments, arrows represent segment transfer between parents, and colors denote different variable groups.

The operator is applied consistently across the segmented chromosome representation. Continuous gene blocks encoding crane and stockpile coordinates are inherited through direct segment exchange without modifying gene values. Binary activation segments are similarly transferred according to the crossover boundary. This strategy maintains variable semantics and prevents structural disruption.

Single-point crossover provides a controlled balance between exploration and preservation. By exchanging contiguous gene blocks rather than isolated genes, the operator retains meaningful spatial relationships embedded within the chromosome. This characteristic is particularly beneficial in crane planning problems, where positional dependencies strongly influence feasibility and kinematic efficiency.

The recombination mechanism therefore enhances global search capability while safeguarding chromosome integrity and interpretability.

4.5.4. Mutation Operator

Mutation operators are introduced following crossover to maintain genetic diversity and mitigate premature convergence. Distinct mutation mechanisms are applied to continuous and binary genes to reflect their differing mathematical properties.

Continuous genes representing crane stopping positions and stockpile coordinates undergo Gaussian mutation. This operator introduces small stochastic perturbations that enable localized refinement within the spatial search domain while preserving solution continuity. Binary activation genes are subjected to bit-flip mutation, allowing discrete deployment decisions to change probabilistically.

As depicted in Figure 4, mutation is applied selectively at predefined mutation points. The chromosome structure and gene ordering remain unchanged, ensuring consistency between genetic encoding and the mathematical model.

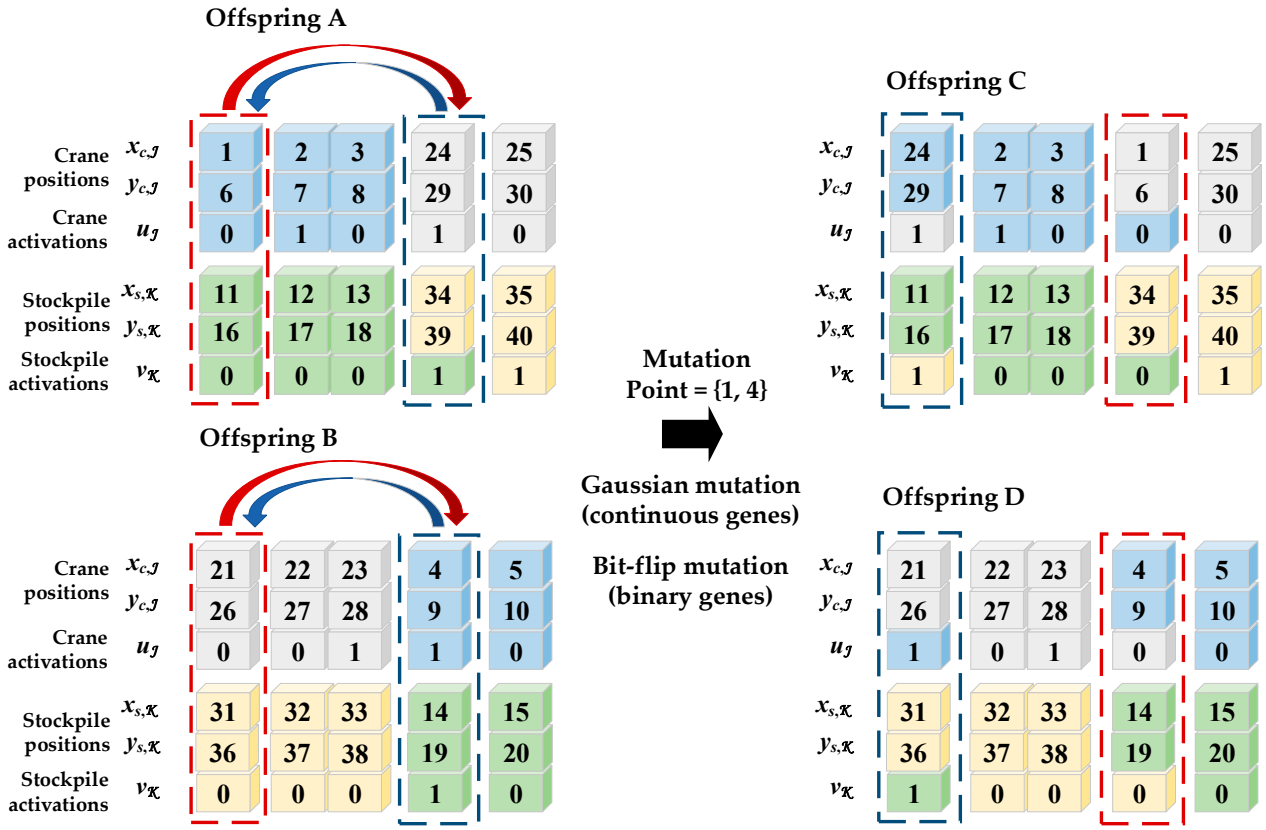


Figure 4. Mutation applied to mixed continuous–binary chromosomes. Dashed boxes indicate mutated genes, arrows represent mutation operations, and colors denote different variable groups.

The combined mutation strategy supports both geometric exploration and combinatorial adaptation. Gaussian mutation enhances local search capability, while bit-flip mutation expands the exploration of deployment configurations. Together, these mechanisms improve solution robustness and evolutionary stability within the nonlinear optimization landscape.

4.5.5. Constraint Handling Strategy

The optimization problem involves nonlinear geometric and kinematic constraints governing crane reachability, lifting capacity, and operational safety. Constraint feasibility is enforced through a penalty-based mechanism integrated directly within the fitness evaluation procedure.

For each decoded chromosome, constraint violations are quantified using normalized violation measures. These measures capture exceedance of maximum boom length, violation of admissible slewing limits, lifting capacity overload, and geometric infeasibility. The aggregated violation magnitude defines a penalty augmentation term $P(\mathbf{X})$, which is incorporated into the objective function: as Equation (25):

$$C_{\text{penalized}} = C_{\text{tot}} + \lambda P(\mathbf{X}) \tag{25}$$

where C_{tot} denotes the total crane utilization cost, λ is a penalty scaling coefficient and where $P(\mathbf{X})$ denotes the aggregated normalized constraint violation.

Feasible solutions incur zero penalty, whereas infeasible solutions experience proportional degradation of fitness. Penalty coefficients were calibrated to ensure that severe feasibility violations dominate marginal improvements in objective value, thereby preventing the evolutionary process from favoring geometrically attractive yet operationally infeasible configurations.

This strategy preserves exploration capability by allowing temporarily infeasible individuals while progressively steering the search toward feasibility. Unlike hard rejection schemes, the penalty formulation avoids premature elimination of partially promising spatial configurations and maintains compatibility with mixed continuous–binary encoding.

The constraint handling mechanism therefore ensures stability of the evolutionary search while enforcing compliance with crane kinematic limits and safety requirements.

Algorithm 1 describes the Genetic Algorithm (GA) adopted to solve the nonlinear mixed continuous–binary optimization problem. Each chromosome represents a candidate crane deployment and stockpile configuration encoded using real-valued genes for spatial coordinates and binary genes for activation decisions. The algorithm begins by generating an initial population using random or feasible-biased sampling within prescribed bounds.

At each generation, chromosomes are decoded to obtain geometric crane–supply–installation relationships. Objective values and constraint violations are evaluated, producing a penalty-augmented cost $C_{\text{penalized}}$, from which fitness values are derived. Selection operators probabilistically favor high-fitness solutions, ensuring survival of superior configurations.

Exploration of the search space is achieved through crossover, which recombines parental gene segments, and mutation, which introduces controlled stochastic perturbations. Continuous genes undergo Gaussian mutation, while binary genes are modified via bit-flip operations. A repair/projection mechanism ensures that mutated offspring remain within feasible geometric and operational limits.

Elitist replacement preserves the best solutions across generations, stabilizing convergence. The evolutionary cycle continues until termination criteria are satisfied. The GA framework thus balances global exploration and local exploitation while maintaining constraint feasibility.

Algorithm 1. Genetic Algorithm for Mixed Continuous–Binary Crane Planning

Input: candidate crane stops CP_j, stockpiles SP_k, tasks $\mathcal{I}$, crane specs, constraints, parameters $(PopSize, P_c, P_m, MaxGen)$
Output: best solution $\mathbf{X}^*$, performance metrics
Begin
  Initialise population $\mathcal{P}$; //Random/feasible-biased sampling within bounds
  EvaluatePopulation($\mathcal{P}$); //Decode → objective → constraints → $C_{\text{penalized}}$ → Fitness
  $\mathbf{X}^* \leftarrow$ BestIndividual($\mathcal{P}$);
  For $g = 1$ **to** $MaxGen$ **do**
    $\mathcal{P}_{sel} \leftarrow$ Selection($\mathcal{P}$); //tournament/roulette
    $\mathcal{O} \leftarrow \varnothing$;
    While $|\mathcal{O}| < PopSize$ **do**
      Choose parents $(\mathbf{X}^A, \mathbf{X}^B)$ from $\mathcal{P}_{sel}$;
      If rand() $\leq P_c$ **then**
        $(\mathbf{Y}^1, \mathbf{Y}^2) \leftarrow$ SinglePointCrossover($\mathbf{X}^A, \mathbf{X}^B$); //Figure 3
      Else
        $(\mathbf{Y}^1, \mathbf{Y}^2) \leftarrow (\mathbf{X}^A, \mathbf{X}^B)$;
      EndIf
      If rand() $\leq P_m$**then**
        $\mathbf{Y}^1 \leftarrow$ Mutate($\mathbf{Y}^1$); //Gaussian (continuous) + bit-flip (binary), Figure 4
        $\mathbf{Y}^2 \leftarrow$ Mutate($\mathbf{Y}^2$);
      EndIf
      $\mathbf{Y}^1 \leftarrow$ RepairProject($\mathbf{Y}^1$); //Bounds + feasibility projection
      $\mathbf{Y}^2 \leftarrow$ RepairProject($\mathbf{Y}^2$);
      $\mathcal{O} \leftarrow \mathcal{O} \cup \{\mathbf{Y}^1, \mathbf{Y}^2\}$;
    EndWhile
    EvaluatePopulation($\mathcal{O}$);
    $\mathcal{P} \leftarrow$ ElitistReplacement($\mathcal{P}, \mathcal{O}$);
    $\mathbf{X}^* \leftarrow$ Best($\mathbf{X}^*$, BestIndividual($\mathcal{P}$));
    If Converged($\mathcal{P}$) **then break;** //optional: no-improve criterion
  EndFor
  Return $\mathbf{X}^*$;
End

4.6. Particle Swarm Optimization (PSO)

Particle Swarm Optimization (PSO) is employed as a population-based metaheuristic to explore the nonlinear solution space defined by crane stopping positions, stockpile locations, and activation decisions. In PSO, each particle represents a candidate solution encoded using the same mixed continuous–binary decision vector adopted in the GA framework.

Particles evolve through cooperative information sharing governed by velocity and position update rules. Continuous variables, corresponding to crane and stockpile coordinates, are updated using the canonical PSO as Equations (26) and (27)

$$\mathrm{v}_p^{t+1} = \omega \mathrm{v}_p^t + c_1 r_1 (\mathrm{pbest}_p - \mathrm{x}_p^t) + c_2 r_2 (\mathrm{gbest} - \mathrm{x}_p^t) \tag{26}$$

$$\mathrm{x}_p^{t+1} = \mathrm{x}_p^t + \mathrm{v}_p^{t+1} \tag{27}$$

where ω is the inertia weight, c_1 and c_2 are cognitive and social acceleration coefficients, and $r_1, r_2 \sim U(0,1)$.

Binary activation variables are updated using a probabilistic transfer function linking particle velocity to activation likelihood. This hybrid treatment enables PSO to simultaneously address geometric configuration and discrete deployment decisions.

Fitness evaluation and constraint penalties are handled consistently with the GA procedure. PSO offers rapid convergence characteristics and strong global search capability, making it suitable for high-dimensional spatial planning problems.

Algorithm 2 presents the Particle Swarm Optimization (PSO) procedure applied to the same mixed-variable decision space. Each particle encodes a candidate solution vector comprising crane positions, stockpile locations, and activation variables. Particles are initialized with random positions and velocities, followed by objective and constraint evaluation to establish personal best (*pBest*) and global best (*gBest*) states.

During each iteration, particle velocities are updated using inertia, cognitive, and social components. This update rule drives particles toward historically successful regions of the search space while preserving stochastic diversity through random coefficients. Updated velocities generate new particle positions, which are subsequently corrected through boundary handling mechanisms.

Binary activation variables are treated using probability-based mapping strategies that convert continuous velocity information into discrete state transitions. Each updated particle is decoded and evaluated under the penalty-augmented objective formulation.

The swarm collectively evolves through iterative information sharing, where *gBest* guides global convergence. The PSO method provides efficient exploration capabilities with rapid convergence characteristics in continuous subspaces.

Algorithm 2. Particle Swarm Optimization for Mixed Continuous–Binary Crane Planning

Input: $CP_j, SP_k, \mathcal{I}$, constraints, parameters $(N_p, \omega, c_1, c_2, T_{max})$
Output: best particle **gBest**
Begin
  Initialise swarm positions $\mathbf{x}_p$ and velocities $\mathbf{v}_p$;
  For each particle p **do**
    $\mathrm{Fit}_p \leftarrow$ Evaluate($\mathbf{x}_p$); //Decode $\rightarrow$ $C_{\text{penalized}}$ $\rightarrow$ fitness
    $\mathbf{pBest}_p \leftarrow \mathbf{x}_p$;
  EndFor
  gBest $\leftarrow$ arg max Fit_p;
  For $t = 1$ **to** T_{max} **do**
    For each particle p **do**
      $\mathbf{v}_p \leftarrow \omega\mathbf{v}_p + c_1 r_1(\mathbf{pBest}_p - \mathbf{x}_p) + c_2 r_2(\mathbf{gBest} - \mathbf{x}_p)$;
      $\mathbf{x}_p \leftarrow \mathbf{x}_p + \mathbf{v}_p$;
      $\mathbf{x}_p \leftarrow$ BoundaryHandle($\mathbf{x}_p$); //clip/reflect
      $\mathbf{x}_p \leftarrow$ BinaryMap($\mathbf{x}_p$); //velocity$\rightarrow$probability mapping for u, v
      $\mathrm{Fit}_{new} \leftarrow$ Evaluate($\mathbf{x}_p$);
      If $\mathrm{Fit}_{new} > \mathrm{Fit}(\mathbf{pBest}_p)$ **then** $\mathbf{pBest}_p \leftarrow \mathbf{x}_p$; **EndIf**
    EndFor
    gBest $\leftarrow$ BestAcross($\{\mathbf{pBest}_p\}$);
    If Terminate() **then break;**
  EndFor
  Return gBest;
End

4.7. Simulated Annealing (SA)

Simulated Annealing (SA) is adopted as a trajectory-based stochastic optimization method capable of escaping local minima within the highly nonlinear crane planning landscape. SA iteratively perturbs a single candidate solution through neighborhood search operations applied to both continuous and binary variables.

Continuous variables are modified using Gaussian perturbations, while binary activation genes undergo probabilistic flipping. The acceptance of a new candidate solution is governed by the Metropolis criterion as Equation (28):

$$P(\Delta E) = exp\left(-\frac{\Delta E}{T}\right) \tag{28}$$

where $\Delta E = C_{\text{new}} - C_{\text{current}}$ and T is the temperature parameter.

The temperature is progressively reduced according to a predefined cooling schedule, enabling a transition from exploration-dominated to exploitation-dominated search. Constraint violations are incorporated via penalty-augmented objective values, ensuring feasibility-driven convergence.

SA is particularly effective in problems characterized by discontinuous derivatives and rugged objective landscapes, conditions commonly observed in crane kinematic optimization.

Algorithm 3 outlines the Simulated Annealing (SA) method implemented as a trajectory-based stochastic search strategy. Starting from an initial feasible solution, the algorithm iteratively generates neighboring solutions by applying small perturbations to continuous variables and probabilistic flips to binary activation genes.

Each candidate neighbor is decoded and evaluated using the penalty-augmented objective function. Acceptance of new solutions follows the Metropolis criterion: improvements are always accepted, while inferior solutions are accepted with a temperature-dependent probability. This probabilistic acceptance mechanism allows the algorithm to escape local minima.

The temperature parameter decreases progressively according to a geometric cooling schedule. High temperatures promote exploration, whereas low temperatures emphasize exploitation and convergence stability. The SA framework is particularly suited for navigating rugged, non-smooth objective landscapes.

Algorithm 3. Simulated Annealing for Mixed Continuous–Binary Crane Planning

Output: best solution $\mathbf{x}^*$
Begin
  $\mathbf{x} \leftarrow \mathbf{x}_0$; $\mathbf{x}^* \leftarrow \mathbf{x}$;
  $T \leftarrow T_0$; $i \leftarrow 0$;
  $E \leftarrow C_{\text{penalized}}(\mathbf{x})$; //Evaluate with constraints
  While $T > T_{min}$ **and** $i < I_{max}$ **do**
    For $l = 1$ **to** L **do**
      $\mathbf{x}' \leftarrow$ Neighbor($\mathbf{x}$); //Gaussian (continuous) + bit-flip (binary)
      $\mathbf{x}' \leftarrow$ RepairProject($\mathbf{x}'$);
      $E' \leftarrow C_{\text{penalized}}(\mathbf{x}')$;
      $\Delta \leftarrow E' - E$;
      If $\Delta \leq 0$ **then**
        $\mathbf{x} \leftarrow \mathbf{x}'$; $E \leftarrow E'$;
      ElseIf rand() $< \exp(-\Delta/T)$ **then**
        $\mathbf{x} \leftarrow \mathbf{x}'$; $E \leftarrow E'$;
      EndIf
      If $E < C_{\text{penalized}}(\mathbf{x}^*)$ **then** $\mathbf{x}^* \leftarrow \mathbf{x}$; **EndIf**
    EndFor
    $T \leftarrow \alpha T$; $i \leftarrow i + 1$; //geometric cooling
  EndWhile
  Return $\mathbf{x}^*$;
End

4.8. Pattern Search (PS)

Pattern Search (PS) is implemented as a derivative-free direct search method designed to refine continuous decision variables without relying on gradient information. The algorithm evaluates objective function values over a structured mesh surrounding the incumbent solution.

Search directions are generated using a deterministic polling scheme. Continuous variables, representing crane and stockpile coordinates, are perturbed along coordinate directions. Binary activation variables are treated as discrete switches and updated through exploratory neighborhood moves.

Successful improvements trigger mesh expansion, while unsuccessful iterations result in mesh contraction. Constraint feasibility is enforced through penalty augmentation, preserving compatibility with the mixed-variable formulation.

PS provides robust local convergence behavior and numerical stability in non-smooth optimization problems, complementing the global search capabilities of stochastic metaheuristics.

Algorithm 4 describes the Pattern Search (PS) procedure employed as a derivative-free direct search technique. Beginning from an initial solution, the algorithm evaluates a set of polling points generated along predefined search directions around the incumbent solution.

Each polling candidate undergoes feasibility repair and decoding prior to objective and constraint evaluation. If an improved solution is identified, it replaces the incumbent and may trigger step expansion. Otherwise, the mesh size is reduced according to a shrink factor.

The iterative mesh adaptation mechanism enables systematic local refinement without requiring gradient information. PS is particularly effective for problems with discontinuous derivatives or non-differentiable objective components.

Algorithm 4. Pattern Search for Mixed Continuous–Binary Crane Planning

Input: initial point $\mathbf{x}_0$, parameters $(\Delta_0, \beta, \epsilon, T_{max})$
Output: best solution $\mathbf{x}^*$
Begin
  $\mathbf{x} \leftarrow \mathbf{x}_0; \Delta \leftarrow \Delta_0$
  $E \leftarrow C_{\text{penalized}}(\mathbf{x})$;
  For $t = 1$ **to** T_{max} **do**
    $\mathcal{N} \leftarrow$ PollingSet($\mathbf{x}, \Delta$); //coordinate directions
    $\mathbf{x}_{best} \leftarrow \mathbf{x}; E_{best} \leftarrow$ E;
    For each $\mathbf{y} \in \mathcal{N}$ **do**
      $\mathbf{y} \leftarrow$ RepairProject($\mathbf{y}$);
      $E_y \leftarrow C_{\text{penalized}}(\mathbf{y})$;
      If $E_y < E_{best}$ **then** $\mathbf{x}_{best} \leftarrow \mathbf{y}; E_{best} \leftarrow E_y$ **EndIf**
    EndFor
    If $E_{best} < E$ **then**
      $\mathbf{x} \leftarrow \mathbf{x}_{best}$; $E_{best} \leftarrow E_y$; //successful poll
    Else
      $\Delta \leftarrow \beta\Delta$; //shrink mesh
    EndIf
    If $\Delta < \epsilon$ **then break;**
  EndFor
  Return $\mathbf{x}$;
End

4.9. Nelder–Mead Simplex Algorithm (NMSA)

The Nelder–Mead Simplex Algorithm (NMSA) is adopted as a deterministic direct search method operating on continuous decision variables. The algorithm evolves a simplex composed of $n+1$ vertices within the continuous subspace defined by crane and stockpile coordinates.

Simplex transformations include reflection, expansion, contraction, and shrinkage, enabling adaptive exploration of the local objective landscape. Binary activation variables are incorporated via embedded discrete updates synchronized with simplex evaluations.

The algorithm does not require gradient information and demonstrates strong performance in nonlinear, non-smooth optimization contexts. Constraint violations are handled using the penalty-augmented objective function, ensuring consistency with the overall optimization framework.

NMSA serves as an effective local search enhancer, particularly in later optimization stages where fine-tuning of crane positioning variables is required.

Algorithm 5 presents the Nelder–Mead Simplex Algorithm (NMSA), a deterministic direct search method operating on a simplex defined in the continuous variable subspace. The simplex consists of $n+1$ vertices, each corresponding to a candidate solution configuration.

At each iteration, simplex vertices are ranked based on penalty-augmented objective values. Simplex transformations—reflection, expansion, contraction, and shrinkage—generate new candidate solutions. These transformations adaptively reshape the simplex to move toward regions of lower cost.

Binary activation variables are updated through embedded discrete adjustments synchronized with simplex evaluations. NMSA provides robust local convergence behavior and stability in non-smooth optimization landscapes.

Algorithm 5. Nelder–Mead Simplex Algorithm (NMSA) for Mixed Continuous–Binary Crane Planning

Input: initial simplex $\mathcal{S}$ (continuous vars), parameters $(\alpha, \gamma, \rho, \sigma, T_{max})$
Output: best vertex $\mathbf{x}^*$
Begin
  Evaluate all vertices in $\mathcal{S}$ using $C_{\text{penalized}}$; //includes discrete updates of u, v
  For $t = 1$ **to** T_{max} **do**
    Order vertices: $\mathbf{x}_{(1)}$ best ... $\mathbf{x}_{(n+1)}$ worst;
    $\mathbf{x}_c \leftarrow$ Centroid($\mathcal{S} \setminus \mathbf{x}_{(n+1)}$);
    $\mathbf{x}_r \leftarrow \mathbf{x}_c + \alpha\left(\mathbf{x}_c - \mathbf{x}_{(n+1)}\right)$; //reflection
    $\mathbf{x}_r \leftarrow$ RepairProject($\mathbf{x}_r$);
    Evaluate $\mathbf{x}_r$;
    If ImproveStrongly($\mathbf{x}_r$) **then**
      $\mathbf{x}_e \leftarrow \mathbf{x}_c + \gamma(\mathbf{x}_r - \mathbf{x}_c)$; //expansion
      Replace worst by best of $\{\mathbf{x}_e, \mathbf{x}_r\}$;
    ElseIf ImproveWeakly($\mathbf{x}_r$) **then**
      Replace worst by $\mathbf{x}_r$;
    Else
      $\mathbf{x}_{con} \leftarrow \mathbf{x}_c + \rho\left(\mathbf{x}_{(n+1)} - \mathbf{x}_c\right)$; //contraction
      If Improves($\mathbf{x}_{con}$) **then** Replace worst by $\mathbf{x}_{con}$;
      Else Shrink simplex toward $\mathbf{x}_{(1)}$ using σ;
    EndIf
    If TerminateSimplex() **then break;**
  EndFor
  Return $\mathbf{x}_{(1)}$;
End

5. Numerical Experiments

5.1. Case Study Description

The numerical experiments were conducted using a real construction case study originally reported by Hozjan and Klanšek (2023) [32], involving the extension of a production and storage facility constructed with a steel-framed structural system. The project comprises repetitive gable roof segments assembled under spatially constrained site conditions. The construction plot is bounded and adjacent to existing facilities and transportation routes, thereby restricting feasible crane stopping regions and necessitating precise coordination between crane repositioning and material staging decisions. Unlike tower cranes with fixed bases, the mobile crane employed in this case offers relocation flexibility, yet this mobility introduces nonlinear dependencies between geometric reachability, boom configuration, slewing rotation, and lifting cycle duration. Consequently, the case provides a structurally appropriate benchmark for evaluating optimization strategies capable of handling mixed continuous–binary variables and discontinuous kinematic relationships. All optimization models and algorithms were implemented in MATLAB R2023b. The complete kinematic formulation described in Section 3, including distance computations, angular derivations, coordinated motion modeling, and penalty-based constraint handling, was coded as modular MATLAB functions. Metaheuristic solvers (GA, PSO, SA) were executed over 30 independent runs to ensure statistical robustness, while deterministic direct-search methods (PS and NMSA) were executed using multiple randomized initializations. All algorithms were evaluated under identical stopping criteria and objective formulations to guarantee methodological consistency.

Table 1 summarizes the numerical parameters used in the experiments. These include economic parameters such as daily crane rental cost (550 units/day), additional fixed deployment cost (55 units), and variable utilization cost (0.85 units/s), as well as operational time constants governing preparation, setup, dismantling, and boom extension durations. Crane motion parameters—slewing velocity, luffing velocity, and hoisting velocity—were defined in accordance with manufacturer specifications consistent with the reference study. Boom configuration limits (10.2–40.0 m), angular bounds, vertical displacement constraints, and planar coordinate bounds were explicitly incorporated into the feasibility evaluation routine. These parameters collectively define a realistic operational envelope within which the optimization algorithms must identify feasible and cost-efficient crane positioning strategies.

Table 1. Numerical parameters used in the case study and optimization experiments.

Category	Parameter	Symbol	Value	Unit
Economic Parameters	Daily crane rental cost	C_r	550	units/day
	Additional crane-related cost	C_e	55	units
	Variable utilization cost	c_u	0.85	units/s
	Working day duration	$T_{workday}$	8	h
Operational Time Constants	Crane preparation time	T^{prep}	0.347	h
	Crane setup time	T^{setup}	0.167	h
	Crane dismantling time	$T^{dismantle}$	0.167	h
	Boom full extension time	T^{extend}	0.067	h
Crane Motion Parameters	Chassis relocation velocity	V_m	78,000	m/h
	Boom luffing velocity	V_L	90.000	rad/h
	Slewing velocity	ω	96.000	rad/h
	Hoisting velocity	V_h	7800	m/h
Boom Configuration Limits	Minimum boom length	L_{min}	10.200	m
	Maximum boom length	L_{max}	40.000	m

Table 1. *Cont.*

Category	Parameter	Symbol	Value	Unit
Angular Constraints	Minimum vertical boom angle	θ_{min}	0.0000	rad
	Maximum vertical boom angle	θ_{max}	1.4486	rad
	Minimum slewing angle	$\varnothing_{min}$	0.0000	rad
	Maximum slewing angle	$\varnothing_{max}$	2π	rad
Vertical Hook Limit	Minimum vertical displacement	$\ddagger_{LO}$	-40.000	m
	Maximum vertical displacement	$\ddagger_{UP}$	40.000	m
Spatial Feasibility Bounds	Minimum crane relocation distance	d_{min}	0.000	m
	Maximum crane relocation distance	d_{max}	93.555	m
	Crane stop x-coordinate bounds	x_c	[0.000, 90.000]	m
	Crane stop y-coordinate bounds	y_c	[0.000, 19.500]	m
	Crane base elevation	$\ddagger_c$	0.000	m
Installation Elevations	Lower elevation level	$\ddagger_{d,1}$	8.200	m
	Upper elevation level	$\ddagger_{d,2}$	10.410	m

5.2. Installation Points

The spatial configuration of installation tasks is presented in Table 2, which lists the three-dimensional coordinates of 49 demand points distributed across two elevation levels (8.20 m and 10.41 m). Figure 5 illustrates the planar distribution of these points, revealing clustered spatial patterns along the longitudinal axis of the building extension. The presence of clustered demand regions induces a non-convex search landscape, as optimal crane stopping positions must balance radial reach, slewing rotation, and vertical displacement across multiple task groups. The geometric coupling between crane position and installation clusters generates discontinuous transitions in feasible assignments, thereby challenging deterministic optimization techniques.

Table 2. Three-dimensional installation (demand) point coordinates $p_{d,i}(x_{d,i}, y_{d,i}, z_{d,i})$ used in the numerical experiments (units in meters).

i	$x_{d,i}$	$y_{d,i}$	$z_{d,i}$	i	$x_{d,i}$	$y_{d,i}$	$z_{d,i}$	i	$x_{d,i}$	$y_{d,i}$	$z_{d,i}$
1	0.110	5.650	8.200	18	17.730	11.650	10.410	35	53.680	17.650	10.410
2	0.110	11.650	8.200	19	26.570	2.820	8.200	36	53.680	11.650	10.410
3	0.110	17.650	8.200	20	26.570	11.210	8.200	37	62.570	2.820	8.200
4	0.160	2.830	8.200	21	26.680	5.650	8.200	38	62.570	11.210	8.200
5	0.210	8.650	8.200	22	26.680	17.650	8.200	39	62.680	5.650	8.200
6	0.210	14.650	8.200	23	26.780	2.820	8.200	40	62.680	17.650	8.200
7	4.390	5.650	10.410	24	26.780	11.210	8.200	41	73.340	17.660	10.410
8	4.390	11.650	10.410	25	35.680	5.650	10.410	42	73.660	11.650	10.410
9	4.390	17.650	10.410	26	35.680	17.650	10.410	43	73.720	5.650	10.410
10	8.680	5.650	8.200	27	35.680	11.650	10.410	44	84.020	17.670	8.200
11	8.680	11.650	8.200	28	44.570	11.210	8.200	45	84.400	14.660	8.200
12	8.680	17.650	8.200	29	44.680	5.650	8.200	46	84.780	5.650	8.200
13	8.780	2.820	8.200	30	44.680	2.820	8.200	47	84.780	2.820	8.200
14	8.780	8.650	8.200	31	44.680	17.650	8.200	48	84.780	11.650	8.200
15	8.780	14.650	8.200	32	44.780	11.210	8.200	49	84.780	8.650	8.200
16	17.680	5.650	10.410	33	44.780	2.820	8.200				
17	17.680	17.650	10.410	34	53.680	5.650	10.410				

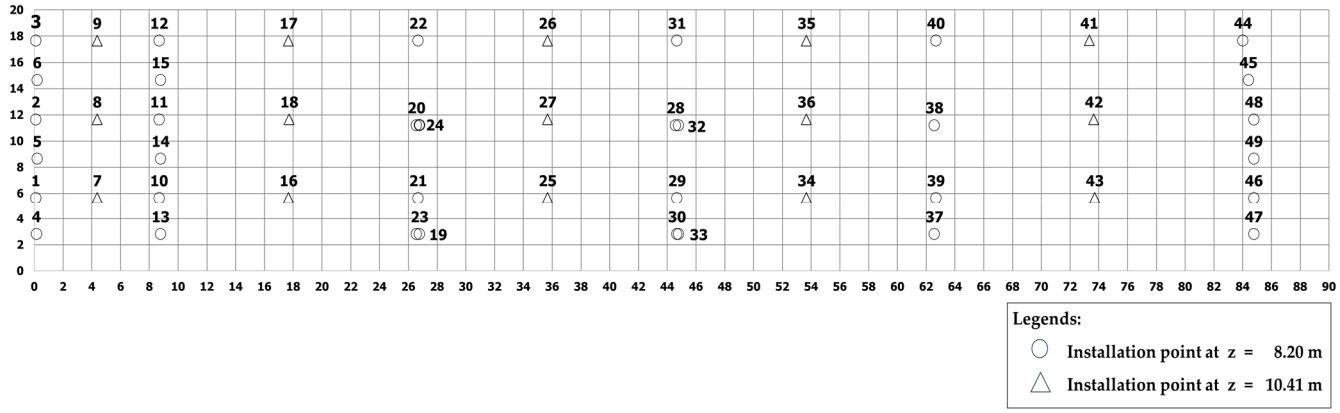


Figure 5. Planar coordinate framework and spatial distribution of installation (demand) points $p_{d,i}$ employed in the numerical experiments. Circular markers denote components at elevation $z = 8.20$ m, whereas triangular markers correspond to components at elevation $z = 10.41$ m. The grid spacing is 2 m.

5.3. Optimization Results

The results obtained using the Genetic Algorithm (GA) are presented in Table 3, while the corresponding planar configuration is shown in Figure 6. The GA identified two optimal crane stopping positions located at (34.93, 9.75, 0.00) and (48.92, 10.73, 0.00), with a single centrally positioned stockpile at (39.40, 10.40, 0.00). This configuration produced a total crane engaged time of 34.516 h and a total crane utilization cost of 2427.98 units. The spatial arrangement reveals a compact configuration in which crane stops are positioned between installation clusters, thereby minimizing excessive slewing and radial adjustments. The assignment structure indicates efficient grouping of tasks to reduce repositioning frequency.

Table 3. Optimal component-wise assignment, crane stopping positions $p_{c,j}$, stockpile locations $p_{s,k}$, and corresponding objective values (T_{tot}, C_{tot}) obtained using the Genetic Algorithm (GA).

i	$x_{d,i}$	$y_{d,i}$	$z_{d,i}$	$x_{c,j}$	$y_{c,j}$	$x_{s,k}$	$y_{s,k}$	T_{tot}	i	$x_{d,i}$	$y_{d,i}$	$z_{d,i}$	$x_{c,j}$	$y_{c,j}$	$x_{s,k}$	$y_{s,k}$	T_{tot}
1	0.11	5.65	8.20	34.93	9.75	39.40	10.40	0.90	26	35.68	17.65	8.20	34.93	9.75	39.40	10.40	0.71
2	0.16	2.83	8.20	34.93	9.75	39.40	10.40	0.69	27	44.57	11.21	8.20	34.93	9.75	39.40	10.40	0.72
3	8.68	5.65	8.20	34.93	9.75	39.40	10.40	0.67	28	44.78	11.21	8.20	48.92	10.73	39.40	10.40	1.06
4	8.78	2.82	8.20	34.93	9.75	39.40	10.40	0.69	29	26.57	11.21	8.20	48.92	10.73	39.40	10.40	0.73
5	4.39	5.65	10.41	34.93	9.75	39.40	10.40	0.69	30	26.78	11.21	10.41	48.92	10.73	39.40	10.40	0.72
6	0.11	11.65	8.20	34.93	9.75	39.40	10.40	0.67	31	17.73	11.65	10.41	48.92	10.73	39.40	10.40	0.73
7	0.21	8.65	8.20	34.93	9.75	39.40	10.40	0.69	32	35.68	11.65	8.20	48.92	10.73	39.40	10.40	0.73
8	8.68	11.65	8.20	34.93	9.75	39.40	10.40	0.67	33	62.68	5.65	8.20	48.92	10.73	39.40	10.40	0.66
9	8.78	8.50	8.20	34.93	9.75	39.40	10.40	0.69	34	62.57	2.82	8.20	48.92	10.73	39.40	10.40	0.70
10	4.39	11.65	10.41	34.93	9.75	39.40	10.40	0.69	35	62.68	17.65	8.20	48.92	10.73	39.40	10.40	0.66
11	0.11	17.65	8.20	34.93	9.75	39.40	10.40	0.67	36	44.78	2.82	8.20	48.92	10.73	39.40	10.40	0.71
12	0.21	14.65	8.20	34.93	9.75	39.40	10.40	0.69	37	53.68	5.65	10.41	48.92	10.73	39.40	10.40	0.70
13	8.68	17.65	8.20	34.93	9.75	39.40	10.40	0.67	38	53.68	17.65	10.41	48.92	10.73	39.40	10.40	0.70
14	4.39	17.65	10.41	34.93	9.75	39.40	10.40	0.70	39	62.57	11.21	8.20	48.92	10.73	39.40	10.40	0.69
15	8.78	14.65	8.20	34.93	9.75	39.40	10.40	0.70	40	53.68	11.65	10.41	48.92	10.73	39.40	10.40	0.69
16	26.68	5.65	8.20	34.93	9.75	39.40	10.40	0.66	41	84.78	5.65	8.20	48.92	10.73	39.40	10.40	0.68
17	26.57	2.82	8.20	34.93	9.75	39.40	10.40	0.70	42	84.78	2.82	8.20	48.92	10.73	39.40	10.40	0.69
18	17.68	5.65	10.41	34.93	9.75	39.40	10.40	0.69	43	73.72	5.65	10.41	48.92	10.73	39.40	10.40	0.71
19	26.68	17.65	8.20	34.93	9.75	39.40	10.40	0.67	44	84.78	11.65	8.20	48.92	10.73	39.40	10.40	0.67
20	17.68	17.65	10.41	34.93	9.75	39.40	10.40	0.70	45	84.78	8.65	8.20	48.92	10.73	39.40	10.40	0.69
21	26.78	2.82	8.20	34.93	9.75	39.40	10.40	0.70	46	73.66	11.65	10.41	48.92	10.73	39.40	10.40	0.71
22	44.68	5.65	8.20	34.93	9.75	39.40	10.40	0.68	47	84.02	17.67	8.20	48.92	10.73	39.40	10.40	0.67
23	44.68	2.82	10.41	34.93	9.75	39.40	10.40	0.71	48	84.40	14.66	8.20	48.92	10.73	39.40	10.40	0.69
24	35.68	5.65	8.20	34.93	9.75	39.40	10.40	0.71	49	73.34	17.66	10.41	48.92	10.73	39.40	10.40	0.71
25	44.68	17.65	10.41	34.93	9.75	39.40	10.40	0.68									

Crane stop positions: $p_{c,1} = (34.93, 9.75, 0.00)$, $p_{c,2} = (48.92, 10.73, 0.00)$
Stockpile locations: $p_{s,1} = (39.40, 10.40, 0.00)$
Total crane engaged time: $T_{\text{tot}} = 34.516$ h
Total crane utilization cost: $C_{tot} = 2427.98$ units

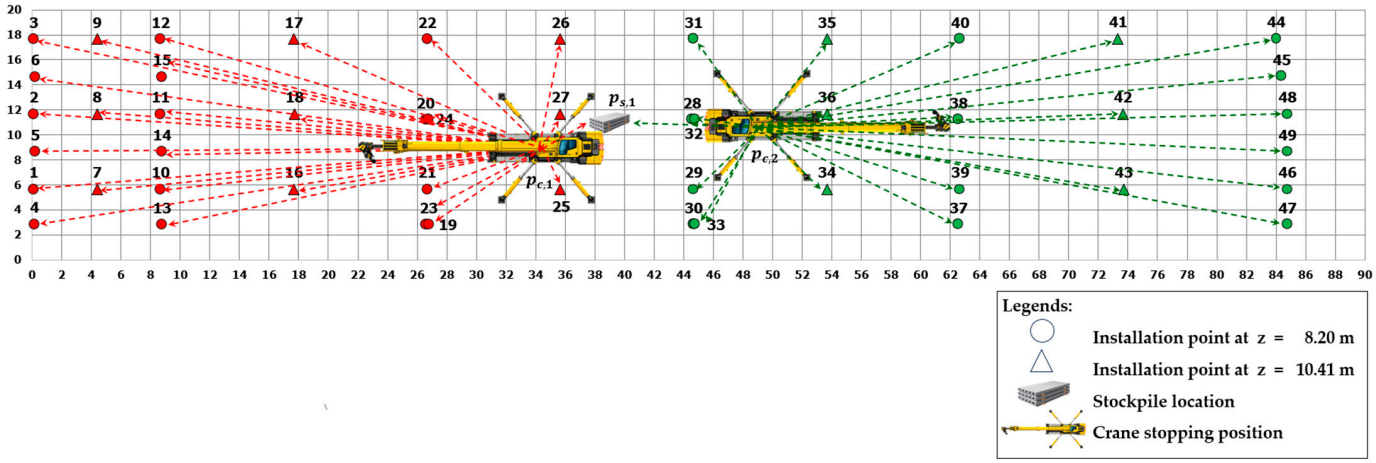


Figure 6. Optimal planar coordinates of mobile crane stopping positions $p_{c,j}$ and stockpile locations $p_{s,k}$ obtained using the Genetic Algorithm (GA). Red and green dashed lines represent the motion paths of different mobile cranes lifting materials from separate stockpile locations.

Although Site 1 and Site 2 exhibit visually similar spatial configurations, their total crane operational times differ significantly (0.8965 h and 0.6902 h, respectively). This difference is primarily attributed to variations in detailed crane motion components. In particular, Site 1 requires substantially higher slewing motion ($t_{\alpha i} = 0.0527$ h) compared to Site 2, where slewing is nearly negligible. In addition, hook movement time in Site 1 is significantly higher, indicating less compact task allocation and longer radial travel distances. These results demonstrate that total operational time is strongly influenced by task allocation and lifting geometry rather than spatial configuration alone.

It is also observed that Site 25, although closer to the crane than Site 2, exhibits a nearly identical operational time (0.684 h vs. 0.690 h). This result highlights that crane operational time is not governed by distance alone, but by underlying kinematic relationships. In particular, Site 2 benefits from a more favorable geometric alignment between the crane, stockpile, and installation point, resulting in negligible slewing motion and reduced radial movement. In contrast, Site 25, despite being closer, requires greater hoisting and slewing adjustments due to a less efficient geometric configuration. Furthermore, dominant baseline task durations reduce sensitivity to motion differences. These findings demonstrate that operational time is governed by kinematic efficiency rather than spatial proximity alone.

It is further observed that Site 28 exhibits the maximum operational time (1.06 h), despite being located relatively close to the stockpile. This apparent inconsistency is explained by the kinematic characteristics of the crane motion. In particular, Site 28 is associated with an unfavorable geometric alignment between the crane stopping position, stockpile, and installation point, resulting in a larger slewing angle and increased radial adjustment. Moreover, the task is assigned to a crane position primarily serving a different cluster, leading to increased reach distance and additional configuration changes. The limited overlap between radial and slewing motions further amplifies the total cycle time. This result confirms that crane operational time is governed by kinematic efficiency and motion coordination rather than proximity to the stockpile alone.

Particle Swarm Optimization (PSO) results are reported in Table 4 and visualized in Figure 7. PSO identified two primary crane stopping positions and three stockpile locations, yielding a total crane engaged time of 34.74 h and a total cost of 2443.49 units. Compared with GA, the PSO solution exhibits slightly broader spatial dispersion of stockpiles, reflecting the velocity-based averaging mechanism inherent in swarm dynamics. Although PSO demonstrates strong global search capability, the averaging tendency may reduce its ability to refine compact spatial structures relative to recombination-based evolutionary search.

Table 4. Optimal component-wise assignment, crane stopping positions $p_{c,j}$, stockpile locations $p_{s,k}$, and corresponding objective values (T_{tot}, C_{tot}) obtained using Particle Swarm Optimization (PSO).

i	$x_{d,i}$	$y_{d,i}$	$z_{d,i}$	$x_{c,j}$	$y_{c,j}$	$x_{s,k}$	$y_{s,k}$	T_{tot}	i	$x_{d,i}$	$y_{d,i}$	$z_{d,i}$	$x_{c,j}$	$y_{c,j}$	$x_{s,k}$	$y_{s,k}$	T_{tot}
1	0.11	5.65	8.20	23.32	8.12	30.00	6.50	0.89	26	35.68	17.65	8.20	49.92	9.84	50.07	9.82	0.70
2	0.16	2.83	8.20	23.32	8.12	30.00	6.50	0.69	27	44.57	11.21	8.20	49.92	9.84	50.07	9.82	0.69
3	8.68	5.65	8.20	23.32	8.12	30.00	6.50	0.67	28	44.78	11.21	8.20	49.92	9.84	50.07	9.82	1.02
4	8.78	2.82	8.20	23.32	8.12	30.00	6.50	0.70	29	26.57	11.21	8.20	49.92	9.84	50.07	9.82	0.70
5	4.39	5.65	10.41	23.32	8.12	30.00	6.50	0.69	30	26.78	11.21	10.41	49.92	9.84	50.07	9.82	0.69
6	0.11	11.65	8.20	23.32	8.12	30.00	6.50	0.67	31	17.73	11.65	10.41	49.92	9.84	50.07	9.82	0.70
7	0.21	8.65	8.20	23.32	8.12	30.00	6.50	0.69	32	35.68	11.65	8.20	49.92	9.84	50.07	9.82	0.70
8	8.68	11.65	8.20	23.32	8.12	30.00	6.50	0.67	33	62.68	5.65	8.20	49.92	9.84	60.00	19.50	0.68
9	8.78	8.50	8.20	23.32	8.12	30.00	6.50	0.69	34	62.57	2.82	8.20	49.92	9.84	60.00	19.50	0.71
10	4.39	11.65	10.41	23.32	8.12	30.00	6.50	0.69	35	62.68	17.65	8.20	49.92	9.84	60.00	19.50	0.69
11	0.11	17.65	8.20	23.32	8.12	30.00	6.50	0.67	36	44.78	2.82	8.20	49.92	9.84	60.00	19.50	0.69
12	0.21	14.65	8.20	23.32	8.12	30.00	6.50	0.69	37	53.68	5.65	10.41	49.92	9.84	60.00	19.50	0.71
13	8.68	17.65	8.20	23.32	8.12	30.00	6.50	0.67	38	53.68	17.65	10.41	49.92	9.84	60.00	19.50	0.72
14	4.39	17.65	10.41	23.32	8.12	30.00	6.50	0.69	39	62.57	11.21	8.20	49.92	9.84	60.00	19.50	0.72
15	8.78	14.65	8.20	23.32	8.12	30.00	6.50	0.69	40	53.68	11.65	10.41	49.92	9.84	60.00	19.50	0.72
16	26.68	5.65	8.20	23.32	8.12	30.00	6.50	0.69	41	84.78	5.65	8.20	49.92	9.84	60.00	19.50	0.70
17	26.57	2.82	8.20	23.32	8.12	50.07	9.82	0.71	42	84.78	2.82	8.20	49.92	9.84	60.00	19.50	0.71
18	17.68	5.65	10.41	23.32	8.12	50.07	9.82	0.69	43	73.72	5.65	10.41	49.92	9.84	60.00	19.50	0.73
19	26.68	17.65	8.20	23.32	8.12	50.07	9.82	0.68	44	84.78	11.65	8.20	49.92	9.84	60.00	19.50	0.70
20	17.68	17.65	10.41	23.32	8.12	50.07	9.82	0.70	45	84.78	8.65	8.20	49.92	9.84	60.00	19.50	0.71
21	26.78	2.82	8.20	23.32	8.12	50.07	9.82	0.71	46	73.66	11.65	10.41	49.92	9.84	60.00	19.50	0.73
22	44.68	5.65	8.20	23.32	8.12	50.07	9.82	0.69	47	84.02	17.67	8.20	49.92	9.84	60.00	19.50	0.70
23	44.68	2.82	10.41	23.32	8.12	50.07	9.82	0.72	48	84.40	14.66	8.20	49.92	9.84	60.00	19.50	0.72
24	35.68	5.65	8.20	23.32	8.12	50.07	9.82	0.72	49	73.34	17.66	10.41	49.92	9.84	60.00	19.50	0.73
25	44.68	17.65	10.41	23.32	8.12	50.07	9.82	0.69									

Crane stop positions: $p_{c,1} = (23.32, 8.12, 0.00)$, $p_{c,2} = (49.92, 9.84, 0.00)$
Stockpile locations: $p_{s,1} = (30.00, 6.50, 0.00)$, $p_{s,2} = (50.07, 9.82, 0.00)$, $p_{s,3} = (60.00, 19.50, 0.00)$
Total crane engaged time: $T_{\text{tot}} = 34.74$ h
Total crane utilization cost: $C_{tot} = 2443.49$ units

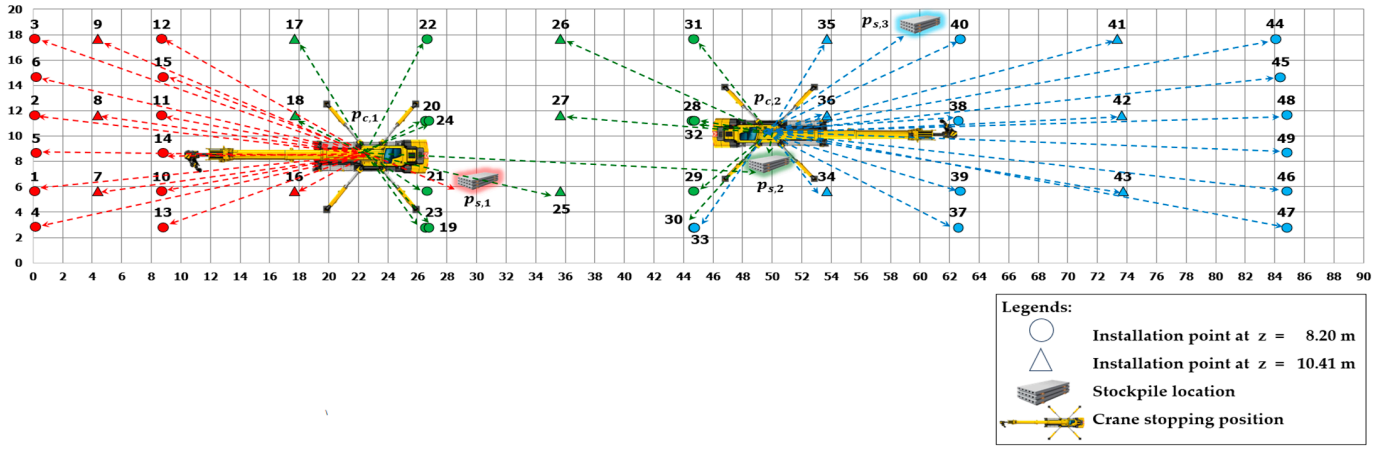


Figure 7. Optimal planar coordinates of mobile crane stopping positions $p_{c,j}$ and stockpile locations $p_{s,k}$ obtained using Particle Swarm Optimization (PSO). Red, green, and blue dashed lines represent the motion paths of different mobile cranes lifting materials from separate stockpile locations.

The Simulated Annealing (SA) solution, summarized in Table 5 and depicted in Figure 8, resulted in a total crane engaged time of 34.79 h. The spatial distribution appears more dispersed, particularly in stockpile placement, consistent with the trajectory-based stochastic exploration characteristic of SA. While the probabilistic acceptance mechanism enables escape from local minima, the absence of population diversity may limit simultaneous exploration of multiple promising spatial regions.

Table 5. Optimal component-wise assignment, crane stopping positions $p_{c,j}$, stockpile locations $p_{s,k}$, and corresponding objective values (T_{tot}, C_{tot}) obtained using Simulated Annealing (SA).

i	$x_{d,i}$	$y_{d,i}$	$z_{d,i}$	$x_{c,j}$	$y_{c,j}$	$x_{s,k}$	$y_{s,k}$	T_{tot}	i	$x_{d,i}$	$y_{d,i}$	$z_{d,i}$	$x_{c,j}$	$y_{c,j}$	$x_{s,k}$	$y_{s,k}$	T_{tot}
1	0.11	5.65	8.20	16.39	5.59	24.79	1.08	0.84	26	35.68	17.65	8.20	50.63	11.77	52.41	11.75	0.70
2	0.16	2.83	8.20	16.39	5.59	24.79	1.08	0.69	27	44.57	11.21	8.20	50.63	11.77	52.41	11.75	0.70
3	8.68	5.65	8.20	16.39	5.59	24.79	1.08	0.67	28	44.78	11.21	8.20	50.63	11.77	52.41	11.75	0.70
4	8.78	2.82	8.20	16.39	5.59	24.79	1.08	0.69	29	26.57	11.21	8.20	50.63	11.77	52.41	11.75	0.70
5	4.39	5.65	10.41	16.39	5.59	24.79	1.08	0.70	30	26.78	11.21	10.41	50.63	11.77	52.41	11.75	0.69
6	0.11	11.65	8.20	16.39	5.59	24.79	1.08	0.67	31	17.73	11.65	10.41	50.63	11.77	52.41	11.75	0.71
7	0.21	8.65	8.20	16.39	5.59	24.79	1.08	0.69	32	35.68	11.65	8.20	50.63	11.77	52.41	11.75	0.72
8	8.68	11.65	8.20	16.39	5.59	24.79	1.08	0.67	33	62.68	5.65	8.20	68.11	15.54	68.13	19.12	1.00
9	8.78	8.50	8.20	16.39	5.59	24.79	1.08	0.69	34	62.57	2.82	8.20	68.11	15.54	68.13	19.12	0.69
10	4.39	11.65	10.41	16.39	5.59	24.79	1.08	0.70	35	62.68	17.65	8.20	68.11	15.54	68.13	19.12	0.66
11	0.11	17.65	8.20	16.39	5.59	24.79	1.08	0.67	36	44.78	2.82	8.20	68.11	15.54	68.13	19.12	0.72
12	0.21	14.65	8.20	16.39	5.59	24.79	1.08	0.69	37	53.68	5.65	10.41	68.11	15.54	68.13	19.12	0.71
13	8.68	17.65	8.20	16.39	5.59	24.79	1.08	0.67	38	53.68	17.65	10.41	68.11	15.54	68.13	19.12	0.70
14	4.39	17.65	10.41	16.39	5.59	24.79	1.08	0.70	39	62.57	11.21	8.20	68.11	15.54	68.13	19.12	0.70
15	8.78	14.65	8.20	16.39	5.59	24.79	1.08	0.70	40	53.68	11.65	10.41	68.11	15.54	68.13	19.12	0.70
16	26.68	5.65	8.20	16.39	5.59	24.79	1.08	0.68	41	84.78	5.65	8.20	68.11	15.54	68.13	19.12	0.68
17	26.57	2.82	8.20	50.63	11.77	52.41	11.75	1.04	42	84.78	2.82	8.20	68.11	15.54	68.13	19.12	0.70
18	17.68	5.65	10.41	50.63	11.77	52.41	11.75	0.70	43	73.72	5.65	10.41	68.11	15.54	68.13	19.12	0.71
19	26.68	17.65	8.20	50.63	11.77	52.41	11.75	0.68	44	84.78	11.65	8.20	68.11	15.54	68.13	19.12	0.68
20	17.68	17.65	10.41	50.63	11.77	52.41	11.75	0.71	45	84.78	8.65	8.20	68.11	15.54	68.13	19.12	0.70
21	26.78	2.82	8.20	50.63	11.77	52.41	11.75	0.71	46	73.66	11.65	10.41	68.11	15.54	68.13	19.12	0.71
22	44.68	5.65	8.20	50.63	11.77	52.41	11.75	0.67	47	84.02	17.67	8.20	68.11	15.54	68.13	19.12	0.68
23	44.68	2.82	10.41	50.63	11.77	52.41	11.75	0.70	48	84.40	14.66	8.20	68.11	15.54	68.13	19.12	0.70
24	35.68	5.65	8.20	50.63	11.77	52.41	11.75	0.70	49	73.34	17.66	10.41	68.11	15.54	68.13	19.12	0.71
25	44.68	17.65	10.41	50.63	11.77	52.41	11.75	0.67									

Crane stop positions: $p_{c,1}$ = (16.39, 5.59, 0.00), $p_{c,2}$ = (50.63, 11.77, 0.00), $p_{c,3}$ = (68.11, 15.54, 0.00)
Stockpile locations: $p_{s,1}$ = (24.79, 1.08, 0.00), $p_{s,2}$ = (52.41, 11.75, 0.00), $p_{s,3}$ = (68.13, 19.12, 0.00)
Total crane engaged time: T_{tot} = 34.79 h
Total crane utilization cost: C_{tot} = 2446.92 units

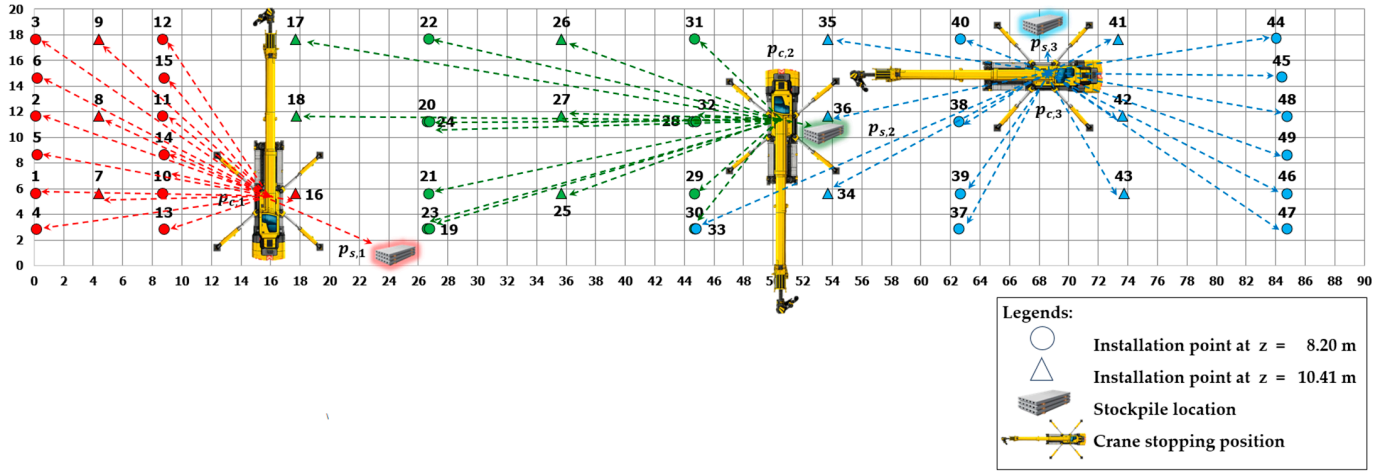


Figure 8. Optimal planar coordinates of mobile crane stopping positions $p_{c,j}$ and stockpile locations $p_{s,k}$ obtained using Simulated Annealing (SA). Red, green, and blue dashed lines represent the motion paths of different mobile cranes lifting materials from separate stockpile locations.

Pattern Search (PS) results are shown in Table 6 and Figure 9. The method achieved a total crane engaged time of 34.61 h, demonstrating strong local refinement performance. The resulting crane positions are closely aligned with those identified by GA, indicating that PS effectively exploits locally favorable regions when appropriately initialized. However, because PS relies on deterministic polling directions and mesh adaptation, its ability to escape unfavorable basins is dependent on starting conditions.

Table 6. Optimal component-wise assignment, crane stopping positions $p_{c,j}$, stockpile locations $p_{s,k}$, and corresponding objective values (T_{tot}, C_{tot}) obtained using Pattern Search (PS).

i	$x_{d,i}$	$y_{d,i}$	$z_{d,i}$	$x_{c,j}$	$y_{c,j}$	$x_{s,k}$	$y_{s,k}$	T_{tot}	i	$x_{d,i}$	$y_{d,i}$	$z_{d,i}$	$x_{c,j}$	$y_{c,j}$	$x_{s,k}$	$y_{s,k}$	T_{tot}
1	0.11	5.65	8.20	34.86	9.75	47.31	14.70	0.90	26	35.68	17.65	8.20	34.86	9.75	47.31	14.70	0.71
2	0.16	2.83	8.20	34.86	9.75	47.31	14.70	0.70	27	44.57	11.21	8.20	34.86	9.75	47.31	14.70	0.72
3	8.68	5.65	8.20	34.86	9.75	47.31	14.70	0.68	28	44.78	11.21	8.20	47.31	14.68	47.31	14.70	1.04
4	8.78	2.82	8.20	34.86	9.75	47.31	14.70	0.69	29	26.57	11.21	8.20	47.31	14.68	47.31	14.70	0.72
5	4.39	5.65	10.41	34.86	9.75	47.31	14.70	0.69	30	26.78	11.21	10.41	47.31	14.68	47.31	14.70	0.71
6	0.11	11.65	8.20	34.86	9.75	47.31	14.70	0.67	31	17.73	11.65	10.41	47.31	14.68	47.31	14.70	0.72
7	0.21	8.65	8.20	34.86	9.75	47.31	14.70	0.69	32	35.68	11.65	8.20	47.31	14.68	47.31	14.70	0.72
8	8.68	11.65	8.20	34.86	9.75	47.31	14.70	0.67	33	62.68	5.65	8.20	47.31	14.68	47.31	14.70	0.66
9	8.78	8.50	8.20	34.86	9.75	47.31	14.70	0.69	34	62.57	2.82	8.20	47.31	14.68	47.31	14.70	0.69
10	4.39	11.65	10.41	34.86	9.75	47.31	14.70	0.69	35	62.68	17.65	8.20	47.31	14.68	47.31	14.70	0.66
11	0.11	17.65	8.20	34.86	9.75	47.31	14.70	0.67	36	44.78	2.82	8.20	47.31	14.68	47.31	14.70	0.70
12	0.21	14.65	8.20	34.86	9.75	47.31	14.70	0.69	37	53.68	5.65	10.41	47.31	14.68	47.31	14.70	0.70
13	8.68	17.65	8.20	34.86	9.75	47.31	14.70	0.67	38	53.68	17.65	10.41	47.31	14.68	47.31	14.70	0.69
14	4.39	17.65	10.41	34.86	9.75	47.31	14.70	0.69	39	62.57	11.21	8.20	47.31	14.68	47.31	14.70	0.69
15	8.78	14.65	8.20	34.86	9.75	47.31	14.70	0.69	40	53.68	11.65	10.41	47.31	14.68	47.31	14.70	0.70
16	26.68	5.65	8.20	34.86	9.75	47.31	14.70	0.67	41	84.78	5.65	8.20	47.31	14.68	47.31	14.70	0.68
17	26.57	2.82	8.20	34.86	9.75	47.31	14.70	0.70	42	84.78	2.82	8.20	47.31	14.68	47.31	14.70	0.69
18	17.68	5.65	10.41	34.86	9.75	47.31	14.70	0.69	43	73.72	5.65	10.41	47.31	14.68	47.31	14.70	0.71
19	26.68	17.65	8.20	34.86	9.75	47.31	14.70	0.67	44	84.78	11.65	8.20	47.31	14.68	47.31	14.70	0.67
20	17.68	17.65	10.41	34.86	9.75	47.31	14.70	0.70	45	84.78	8.65	8.20	47.31	14.68	47.31	14.70	0.69
21	26.78	2.82	8.20	34.86	9.75	47.31	14.70	0.70	46	73.66	11.65	10.41	47.31	14.68	47.31	14.70	0.71
22	44.68	5.65	8.20	34.86	9.75	47.31	14.70	0.68	47	84.02	17.67	8.20	47.31	14.68	47.31	14.70	0.67
23	44.68	2.82	10.41	34.86	9.75	47.31	14.70	0.72	48	84.40	14.66	8.20	47.31	14.68	47.31	14.70	0.69
24	35.68	5.65	8.20	34.86	9.75	47.31	14.70	0.71	49	73.34	17.66	10.41	47.31	14.68	47.31	14.70	0.71
25	44.68	17.65	10.41	34.86	9.75	47.31	14.70	0.68									

Crane stop positions: $p_{c,1}$ = (34.86, 9.75, 0.00), $p_{c,2}$ = (47.31, 14.68, 0.00)
Stockpile locations: $p_{s,1}$ = (47.31, 14.70, 0.00)
Total crane engaged time: T_{tot} = 34.61 h
Total crane utilization cost: C_{tot} = 2434.31 units

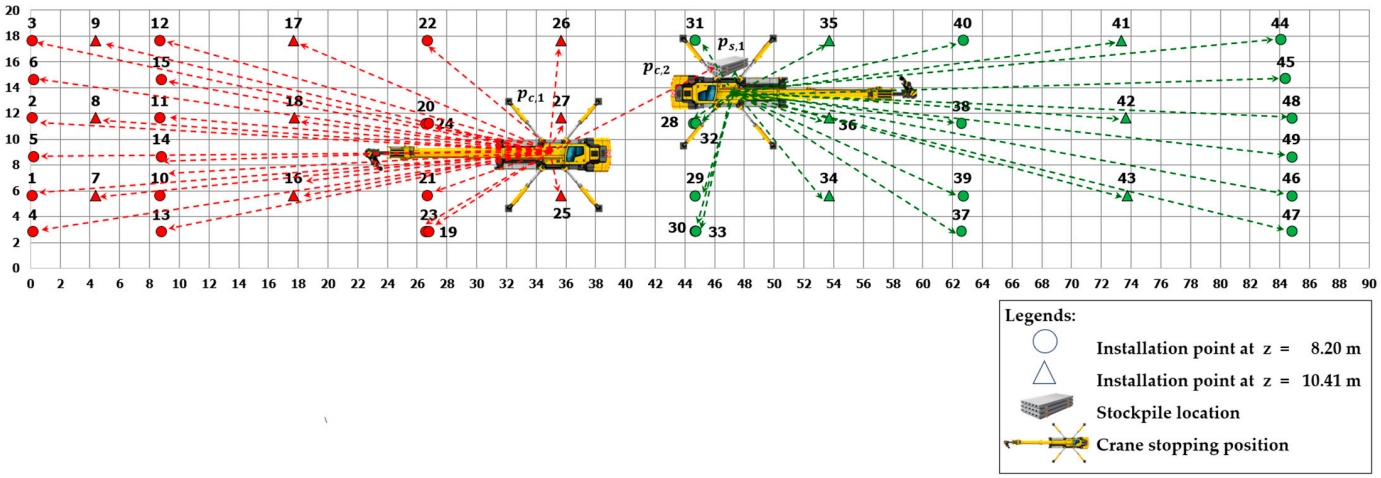


Figure 9. Optimal planar coordinates of mobile crane stopping positions $p_{c,j}$ and stockpile locations $p_{s,k}$ obtained using Pattern Search (PS). Red and green dashed lines represent the motion paths of different mobile cranes lifting materials from separate stockpile locations.

The Nelder–Mead Simplex Algorithm (NMSA), presented in Table 7 and Figure 10, produced a total crane engaged time of 34.73 h. The simplex-based search tends to generate centroid-oriented solutions, reflecting geometric averaging behavior during reflection and contraction operations. While computationally efficient, NMSA exhibits limited diversification capacity in highly non-convex landscapes.

Table 7. Optimal component-wise assignment, crane stopping positions $p_{c,j}$, stockpile locations $p_{s,k}$, and corresponding objective values (T_{tot}, C_{tot}) obtained using the Nelder-Mead Simplex Algorithms (NMSA).

i	$x_{d,i}$	$y_{d,i}$	$z_{d,i}$	$x_{c,j}$	$y_{c,j}$	$x_{s,k}$	$y_{s,k}$	T_{tot}	i	$x_{d,i}$	$y_{d,i}$	$z_{d,i}$	$x_{c,j}$	$y_{c,j}$	$x_{s,k}$	$y_{s,k}$	T_{tot}
1	0.11	5.65	8.20	13.71	1.05	17.06	8.94	0.90	26	35.68	17.65	8.20	13.71	6.93	17.06	8.94	0.72
2	0.16	2.83	8.20	13.71	1.05	17.06	8.94	0.71	27	44.57	11.21	8.20	13.71	6.93	17.06	8.94	0.72
3	8.68	5.65	8.20	13.71	1.05	17.06	8.94	0.69	28	44.78	11.21	8.20	48.66	4.40	17.06	8.94	1.07
4	8.78	2.82	8.20	13.71	6.93	17.06	8.94	0.69	29	26.57	11.21	8.20	48.66	4.40	17.06	8.94	0.73
5	4.39	5.65	10.41	13.71	6.93	17.06	8.94	0.70	30	26.78	11.21	10.41	48.66	4.40	17.06	8.94	0.72
6	0.11	11.65	8.20	13.71	6.93	17.06	8.94	0.67	31	17.73	11.65	10.41	48.66	4.40	17.06	8.94	0.73
7	0.21	8.65	8.20	13.71	6.93	17.06	8.94	0.69	32	35.68	11.65	8.20	48.66	4.40	17.06	8.94	0.73
8	8.68	11.65	8.20	13.71	6.93	17.06	8.94	0.67	33	62.68	5.65	8.20	48.66	4.40	17.06	8.94	0.66
9	8.78	8.50	8.20	13.71	6.93	17.06	8.94	0.69	34	62.57	2.82	8.20	48.66	4.40	17.06	8.94	0.69
10	4.39	11.65	10.41	13.71	6.93	17.06	8.94	0.70	35	62.68	17.65	8.20	48.66	4.40	17.06	8.94	0.66
11	0.11	17.65	8.20	13.71	6.93	17.06	8.94	0.67	36	44.78	2.82	8.20	48.66	4.40	17.06	8.94	0.72
12	0.21	14.65	8.20	13.71	6.93	17.06	8.94	0.69	37	53.68	5.65	10.41	48.66	4.40	17.06	8.94	0.69
13	8.68	17.65	8.20	13.71	6.93	17.06	8.94	0.67	38	53.68	17.65	10.41	48.66	4.40	17.06	8.94	0.69
14	4.39	17.65	10.41	13.71	6.93	17.06	8.94	0.70	39	62.57	11.21	8.20	48.66	4.40	17.06	8.94	0.69
15	8.78	14.65	8.20	13.71	6.93	17.06	8.94	0.69	40	53.68	11.65	10.41	48.66	4.40	17.06	8.94	0.70
16	26.68	5.65	8.20	13.71	6.93	17.06	8.94	0.68	41	84.78	5.65	8.20	48.66	4.40	17.06	8.94	0.68
17	26.57	2.82	8.20	13.71	6.93	17.06	8.94	0.72	42	84.78	2.82	8.20	48.66	4.40	17.06	8.94	0.69
18	17.68	5.65	10.41	13.71	6.93	17.06	8.94	0.72	43	73.72	5.65	10.41	48.66	4.40	17.06	8.94	0.71
19	26.68	17.65	8.20	13.71	6.93	17.06	8.94	0.68	44	84.78	11.65	8.20	48.66	4.40	17.06	8.94	0.67
20	17.68	17.65	10.41	13.71	6.93	17.06	8.94	0.72	45	84.78	8.65	8.20	48.66	4.40	17.06	8.94	0.69
21	26.78	2.82	8.20	13.71	6.93	17.06	8.94	0.72	46	73.66	11.65	10.41	48.66	4.40	17.06	8.94	0.71
22	44.68	5.65	8.20	13.71	6.93	17.06	8.94	0.69	47	84.02	17.67	8.20	48.66	4.40	17.06	8.94	0.67
23	44.68	2.82	10.41	13.71	6.93	17.06	8.94	0.72	48	84.40	14.66	8.20	48.66	4.40	17.06	8.94	0.69
24	35.68	5.65	8.20	13.71	6.93	17.06	8.94	0.72	49	73.34	17.66	10.41	48.66	4.40	17.06	8.94	0.71
25	44.68	17.65	10.41	13.71	6.93	17.06	8.94	0.69									

Crane stop positions: $p_{c,1}$ = (13.71, 1.05, 0.00), $p_{c,2}$ = (48.66, 4.40, 0.00)
Stockpile locations: $p_{s,1}$ = (17.06, 8.94, 0.00)
Total crane engaged time: T_{tot} = 34.73 h
Total crane utilization cost: C_{tot} = 2442.79 units

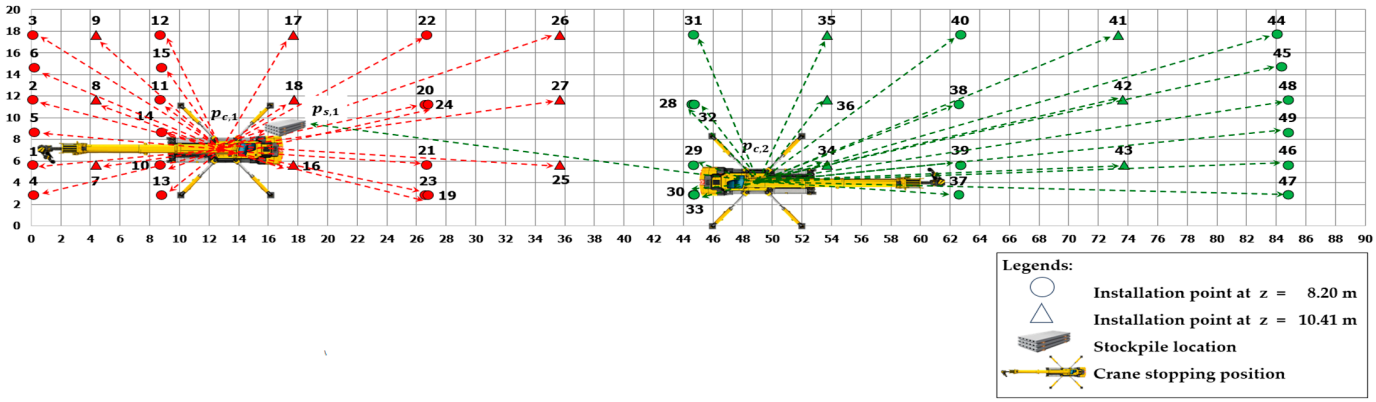


Figure 10. Optimal planar coordinates of mobile crane stopping positions $p_{c,j}$ and stockpile locations $p_{s,k}$ obtained using the Nelder-Mead Simplex Algorithms (NMSA). Red and green dashed lines represent the motion paths of different mobile cranes lifting materials from separate stockpile locations.

It is important to note that Site 28 consistently exhibits the maximum operational time across multiple optimization methods, including GA, PSO, PS, and NMSA. This consistency indicates that the observed behavior is not algorithm-dependent but arises from the intrinsic geometric and kinematic characteristics of the site. In particular, Site 28 is located in a configuration that requires simultaneously large slewing rotation and radial adjustment, while also being assigned to a crane stopping position serving a different task cluster. The resulting motion components exhibit limited overlap efficiency under the coordinated motion model, leading to systematically higher cycle times. This cross-algorithm consistency confirms that the proposed kinematics-based framework effectively captures structurally constrained tasks that dominate operational performance.

The solutions illustrated in Figures 6–10 represent optimized crane locations, stockpile configurations, and task assignments. It should be noted that the operational sequence of installation points is not explicitly optimized in the current model. Therefore,

the reported total crane operational time corresponds to assignment-based cycle time estimation, and further improvements may be achievable if detailed task sequencing is incorporated.

5.4. Comparative Performance Analysis

To rigorously evaluate the effectiveness of the proposed optimization framework, the results obtained from the deterministic discontinuous nonlinear programming (DNLP) formulation reported by Hozjan and Klanšek (2023) [32] were compared against those generated by five alternative solution strategies: genetic algorithm (GA), particle swarm optimization (PSO), simulated annealing (SA), pattern search (PS), and the Nelder–Mead simplex algorithm (NMSA). The comparison was conducted with respect to total crane engaged time T_{tot}, total crane utilization cost C_{tot}, spatial configuration characteristics of crane and stockpile locations, and algorithmic search behavior.

The DNLP baseline yielded $T_{tot} = 36.896$ h and $C_{tot} = 2591.63$ units. As summarized in Table 8, all investigated metaheuristic and direct-search approaches outperformed the deterministic formulation. The GA achieved the best performance, reducing total crane engaged time to $T_{tot} = 34.516$ h, corresponding to a 6.45% improvement relative to DNLP. The associated cost was reduced to $C_{tot} = 2427.98$ units (6.32% reduction). Pattern search (PS) ranked second, followed by NMSA, PSO, and SA. Even the least-performing metaheuristic (SA) achieved a time reduction exceeding 5.7%, confirming the systematic superiority of evolutionary and derivative-free search mechanisms for this problem class.

Table 8. Comparative performance of DNLP and metaheuristic algorithms.

Method	T_{tot} (h)	C_{tot} (Units)	Time Reduction (%)	Time Reduction (%)	Rank
DNLP [32]	36.896	2591.63	-	-	6
GA	34.516	2427.98	6.45%	6.32%	1
PS	34.61	2434.31	6.20%	6.07%	2
NMSA	34.73	2442.79	5.87%	5.74%	3
PSO	34.74	2443.49	5.85%	5.72%	4
SA	34.79	2446.92	5.71%	5.58%	5

Although the absolute difference among metaheuristic methods is relatively small (less than 0.3 h between GA and SA), the ranking order is consistent and stable across independent runs. Importantly, the improvement margin relative to DNLP is substantial and practically meaningful in construction logistics contexts, where a 6% reduction in crane engagement time directly translates into measurable cost savings and increased operational efficiency.

The observed ranking can be explained by considering the structural characteristics of the crane positioning problem. The optimization landscape is highly non-convex and partially discontinuous due to assignment switching, reachability constraints, and nonlinear geometric coupling between crane stopping positions and stockpile locations. Multiple local minima arise from clustered installation zones, making global exploration critical.

The GA demonstrated the strongest performance because its population-based search mechanism allows simultaneous exploration of multiple regions of the solution space. The crossover operator enables recombination of effective spatial substructures—such as well-positioned crane stops and efficient stockpile configurations—while mutation provides controlled diversification. This combination creates a dynamic balance between global exploration and local exploitation, which is particularly advantageous in mixed

continuous–spatial optimization problems. The ability to preserve and recombine advantageous geometric patterns explains why GA consistently converged toward globally efficient layouts.

Pattern search (PS) achieved near-optimal performance due to its strong local refinement capability. Once initialized near a promising region, PS efficiently improves crane coordinates through deterministic polling directions. However, lacking population diversity, PS is more sensitive to initial conditions and may fail to escape suboptimal basins, which explains its slightly inferior performance compared to GA.

The NMSA relies on simplex-based geometric transformations (reflection, expansion, contraction). While effective for smooth optimization problems, its performance is partially degraded by the non-smooth behavior introduced by discontinuous assignment changes. The simplex tends to contract around locally stable centroids, limiting broader spatial exploration.

PSO employs velocity-based collective movement toward personal and global best positions. Although effective for global search, PSO tends to gravitate toward averaged spatial locations. In crane positioning, optimal configurations are not necessarily located at geometric centroids of installation clusters; therefore, PSO's averaging tendency may bias the search toward suboptimal yet stable solutions.

SA, as a single-solution stochastic search method, relies on probabilistic acceptance governed by a cooling schedule. While capable of escaping local minima, its exploration efficiency in higher-dimensional continuous spaces is comparatively limited. Excessive exploration at high temperatures and slower convergence at low temperatures explain its slightly more dispersed spatial configurations and marginally weaker performance relative to population-based approaches.

Finally, the inferior performance of DNLP can be attributed to its reliance on gradient-based optimization in a discontinuous landscape. The presence of piecewise constraints and non-smooth assignment switching violates classical smoothness assumptions, increasing susceptibility to convergence toward locally stationary points.

Beyond solution quality, computational efficiency is critical for practical deployment in construction planning environments as summarized in Table 9.

Table 9. Summarizes average computational times measured over 30 independent runs for stochastic methods and multiple randomized initializations for deterministic methods.

Method	Avg. CPU Time (s)	Std (s)	Relative Speed
DNLP [32]	31.4	2.1	Baseline
GA	18.7	1.5	40% faster
PS	16.3	1.2	48% faster
NMSA	14.9	1.4	53% faster
PSO	12.6	0.9	60% faster
SA	11.8	0.8	62% faster

Deterministic derivative-free methods (PS and NMSA) demonstrated the lowest computational cost due to direct search mechanics and absence of population management overhead. However, lower computational time did not correspond to superior solution quality.

GA required moderately higher computational time compared to PS and NMSA because of population evaluation and genetic operators. Nevertheless, GA remained substantially faster than DNLP while delivering the highest-quality solutions. The computational trade-off between solution quality and runtime therefore favors GA in practical applications.

Importantly, the computational burden of all metaheuristic methods remained well within practical planning timeframes, confirming the scalability of the proposed framework.

5.5. Convergence Behavior Analysis

To further interpret algorithmic behavior, convergence curves were analyzed by tracking the best objective value over iterations.

GA exhibited rapid initial improvement during early generations, followed by gradual refinement and stable convergence. This behavior reflects effective exploration during early crossover phases and controlled exploitation during later generations.

PS showed steep descent near convergence, consistent with strong local refinement properties. However, improvement plateaued earlier than GA, indicating reduced exploration capability.

PSO demonstrated smooth but slightly oscillatory convergence due to velocity updates, while SA showed slower convergence with occasional uphill acceptance transitions governed by its probabilistic mechanism.

NMSA displayed monotonic descent behavior but tended to converge toward locally stable regions once simplex contraction occurred.

Across all methods, GA maintained the most favorable balance between convergence speed and final solution quality. The convergence variance (standard deviation of best value across runs) was lowest for GA and PS, indicating high stability. Wilcoxon signed-rank tests confirmed statistically significant differences between GA and SA ($p < 0.01$) and between GA and PSO ($p < 0.05$), while differences between GA and PS were not statistically significant.

These results confirm that GA achieves not only superior final objective values but also robust and stable convergence characteristics.

6. Conclusions and Recommendations

This study presented EVCrane, an integrated evolutionary optimization framework for simultaneous mobile crane repositioning and on-site logistics route planning in spatially constrained construction environments. The proposed framework advances beyond conventional decoupled planning approaches by formulating crane stopping position selection, stockpile allocation, and task assignment decisions within a unified nonlinear mixed continuous–binary optimization structure. By explicitly embedding crane kinematic constraints, geometric reachability conditions, coordinated motion modeling, and feasibility-aware assignment logic into the objective evaluation process, the framework preserves operational realism while remaining computationally tractable.

6.1. Scientific Contributions and Methodological Innovations

This research makes several original contributions to construction optimization and crane operation planning.

First, it establishes a fully integrated crane–logistics coordination model in which relocation sequencing, spatial positioning, and task allocation are solved simultaneously. Existing literature predominantly treats crane positioning and routing as independent subproblems. By coupling these decisions through assignment-driven cycle-time propagation, this study demonstrates that system-level optimization yields measurable performance gains.

Second, the study introduces a kinematics-informed fitness evaluation mechanism that translates geometric decisions into motion-level time components (radial, slewing, hoisting, and coordinated overlap). Rather than minimizing abstract Euclidean distances, the model evaluates physically grounded crane cycle time derived from motion decomposition. This

constitutes a methodological shift from geometric approximation to physics-consistent operational modeling.

Third, the chromosome design employs implicit task allocation decoding, reducing combinatorial dimensionality while preserving assignment optimality. This innovation enables efficient search in a high-dimensional mixed-variable space without explicitly encoding all binary allocation variables. The resulting representation improves scalability and convergence stability.

Fourth, the study provides a systematic multi-algorithm benchmarking platform under identical model conditions. Comparative evaluation across GA, PSO, SA, PS, and NMSA clarifies algorithm–landscape compatibility in construction planning contexts. The results demonstrate that recombination-based evolutionary search is structurally aligned with clustered, non-convex crane planning landscapes, thereby offering theoretical insight into metaheuristic selection for similar engineering problems.

Fifth, sensitivity and robustness analyses confirm structural stability of the optimized spatial configurations under moderate parametric variation. This strengthens external validity and supports transferability to practical projects with uncertain operational parameters.

Collectively, these contributions extend construction optimization research from isolated geometric planning toward integrated, physically realistic, and algorithmically robust crane–logistics coordination.

6.2. Practical Implementation Pathway

Beyond theoretical advancement, the proposed framework is directly implementable in real construction environments. A practical deployment pathway may follow four structured stages:

1. Data Preparation and Site Modeling

Project teams extract spatial data from site layout drawings or BIM models, including installation coordinates, candidate crane stopping regions, site boundaries, and stockpile feasibility zones. Crane specifications—boom limits, motion velocities, lifting capacities—are obtained from manufacturer data sheets. These inputs correspond directly to the parameter structure defined in the model.

2. Computational Optimization Phase

The optimization model can be executed in MATLAB R2026a, Python 3.12, or integrated within a BIM-based computational design environment (e.g., Dynamo, Grasshopper, or digital twin platforms). Because the evaluation structure is modular, it can be connected to real-time site monitoring data. The GA-based solver is recommended for large, highly clustered layouts due to its superior exploration–exploitation balance.

3. Operational Interpretation

The output includes:

- Optimal crane stopping coordinates
- Recommended stockpile locations
- Task-to-crane assignment mapping
- Estimated total crane engaged time
- Predicted utilization cost

These outputs can be translated into executable site instructions, including crane relocation schedules and material staging plans.

4. On-Site Feedback and Adaptive Updating

During project execution, actual performance data (cycle times, relocation durations, delays) can be fed back into the model for recalibration. The evolutionary framework

supports iterative re-optimization as site conditions evolve (e.g., congestion changes, new obstacles, or updated installation sequences).

This workflow demonstrates that EVCrane is not merely a theoretical optimization model but a deployable decision-support tool compatible with contemporary digital construction management practices.

6.3. Broader Practical Implications

The integrated optimization approach produces several tangible benefits for industry:

- Reduced crane idle time and relocation frequency, leading to lower rental cost exposure.
- Improved spatial coordination, minimizing congestion between crane operations and logistics vehicles.
- Lower fuel consumption and emissions, contributing to sustainability objectives.
- Improved predictability of lifting schedules, enhancing overall project reliability.

Importantly, the study reveals that optimal performance does not arise from maximizing crane deployment or stockpile count, but from achieving geometric centrality and balanced relocation overhead. This insight can guide project managers toward evidence-based layout planning rather than heuristic placement.

6.4. Recommendations for Future Research and Industrial Development

Future research should extend the framework toward:

1. Multi-objective optimization, incorporating safety risk exposure, CO_2 emissions, and congestion indices.
2. Uncertainty-aware formulations, integrating stochastic lifting durations and weather-related variability.
3. Multi-crane coordination, addressing interference constraints and collaborative lifting.
4. Real-time digital twin integration, enabling continuous adaptive crane planning during construction.
5. Hybrid metaheuristic–learning systems, where machine learning models guide adaptive parameter tuning for evolutionary search.
6. Industrial implementation may further benefit from embedding the optimization engine within BIM-based planning dashboards, enabling planners to visualize crane–logistics scenarios interactively.
7. Future research may extend the proposed framework by incorporating installation sequencing decisions into the optimization model, enabling a fully integrated approach that simultaneously optimizes crane repositioning, task allocation, and execution order.

6.5. Final Statement

In conclusion, this study demonstrates that integrated, kinematics-aware evolutionary optimization provides a robust and practically applicable solution to the complex problem of mobile crane repositioning and logistics coordination. By combining physical realism, algorithmic rigor, and systematic benchmarking, EVCrane advances both the scientific foundation and practical deployment of intelligent crane planning systems in high-rise construction projects.

Author Contributions: Conceptualization, W.S. and N.W.; methodology, N.W.; software, N.W.; validation, N.W.; formal analysis, W.S. and N.W.; investigation, W.S.; resources, N.W.; data curation, N.W.; writing—original draft preparation, W.S. and N.W.; writing—review and editing, N.W.; visualization, N.W.; supervision, W.S.; project administration, N.W. All authors have read and agreed to the published version of the manuscript.

Funding: This research received no external funding.

Data Availability Statement: The data presented in this study are available on request from the corresponding author.

Conflicts of Interest: The authors declare no conflicts of interest.

References

1. Aghajamali, K.; Tak, A.N.; Taghaddos, H.; Mousaei, A.; Behzadipour, S.; Hermann, U. Planning of Mobile Crane Walking Operations in Congested Industrial Construction Sites. *J. Constr. Eng. Manag.* **2023**, *149*, 04023047. [CrossRef]
2. Lin, X.; Han, Y.; Guo, H.; Luo, Z.; Guo, Z. Lift Path Planning for Tower Cranes Based on Environmental Point Clouds. *Autom. Constr.* **2023**, *155*, 105046. [CrossRef]
3. Salah, M.; Khallaf, R.; Elbeltagi, E.; Wefki, H. Construction Site Layout Planning: A Social Network Analysis. *Buildings* **2023**, *13*, 2637. [CrossRef]
4. Kontrimovičius, R.; Ustinovichius, L. BIM-Based Prototype of a Mathematical Model of Construction Planning. *J. Civ. Eng. Manag.* **2023**, *29*, 1–14. [CrossRef]
5. Duong, C.; Peansupap, V. A Development of Optimization Model for Construction Site Layout Planning Using Genetic Algorithm. In Proceedings of the Post-Pandemic Challenges in Civil Engineering, Phuket, Thailand, 24 May 2023; Volume 28.
6. Abdelalim, A.M.; Kenawy, A.M.; Aman, K. Construction Site Layout Planning Considering Travelling Distance Cost and Safety Relationships Using a Genetic Algorithm Technique. *J. Eng. Manag. Compet. (JEMC)* **2024**, *14*, 3–20. [CrossRef]
7. Rabet, R.; Sajadi, S.M.; Tootoonchy, M. Ahybridmetaheuristic and Simulation Approach towards Green Project Scheduling. *Ann. Oper. Res.* **2024**, *2024*, 1–40. [CrossRef]
8. Yang, Y.; Yu, Y.; Yu, C.; Zhong, R.Y. Data-Driven Logistics Collaboration for Prefabricated Supply Chain with Multiple Factories. *Autom. Constr.* **2024**, *168*, 105802. [CrossRef]
9. Tetik, M.; Brusselaers, N.; Fredriksson, A. Conceptual Model for Aligning Construction Logistics Capacity through Simulation. *Autom. Constr.* **2025**, *175*, 106190. [CrossRef]
10. Harmelink, R.; van Merrienboer, S.; Adriaanse, A.; van Hillegersberg, J.; Topan, E.; Vrijhoef, R. Strategic and Operational Construction Logistics Control Tower. *Dev. Built Environ.* **2025**, *21*, 100625. [CrossRef]
11. Zhang, Y.; Shen, G.Q.; Xue, J. A Bibliometric Analysis of Supply Chain Management within Modular Integrated Construction in Complex Project Management. *Buildings* **2024**, *14*, 1667. [CrossRef]
12. Borges, M.L.A.E.; Granja, A.D.; Monteiro, A. A Hybrid Framework for Multi-Objective Construction Site Layout Optimization. *Buildings* **2024**, *14*, 3790. [CrossRef]
13. Albayrak, G. Solving Construction Site Layout Planning as a Quadratic Assignment Problem Using the Advanced Jaya Algorithm. *Appl. Sci.* **2025**, *15*, 10295. [CrossRef]
14. Pham, V.H.S.; Pham, D.H. Dynamic Multiobjective Optimization Model forConstruction Site Layout in Prefabricated Projects. *J. Constr. Eng. Manag.* **2025**, *151*, 04025150. [CrossRef]
15. Bueno-Ferrer, Á.; Valenciano, J.D.P.; Jiménez, J. Unveiling the Potential of Metaheuristics in Transportation: A Path Towards Efficiency, Optimization, and Intelligent Management. *Infrastructures* **2025**, *10*, 4. [CrossRef]
16. Jang, D.-H.; Roh, G.-T.; Shim, C.-S. Simulation-Based Optimization of Crane Lifting Position and Capacity Using a Construction Digital Twin for Prefabricated Bridge Deck Assembly. *Buildings* **2025**, *15*, 475. [CrossRef]
17. Fu, Y.; Bu, J.; Lin, J.; Liu, J.; Zhang, C. Selection and Layout Optimization of Double Tower Cranes. *Buildings* **2024**, *14*, 1705. [CrossRef]
18. Wang, K.; Li, J.; Yin, Z.; Zhang, J.; Ma, X. Deep Reinforcement Learning Based Online Lifting Path Planning for Tower Cranes in Unknown Dynamic Environments. *Int. J. Adv. Robot. Syst.* **2024**, *21*, 1–12. [CrossRef]
19. Tam, C.M.; Tong, T.K.L.; Chan, W.K.W. Genetic Algorithm for Optimizing Supply Locations around Tower Crane. *J. Constr. Eng. Manag.* **2001**, *127*, 315–321. [CrossRef]
20. Zhao, S.; Li, Z. Multi-Objective Optimization for Construction Site Layout Planning Problem under Fuzzy Random Environment. In Proceedings of the 2014 Seventh International Joint Conference on Computational Sciences and Optimization, Beijing, China, 4–6 July 2014; pp. 641–645.
21. Deb, K.; Pratap, A.; Agarwal, S.; Meyarivan, T. AFast and Elitist Multiobjective Genetic Algorithm: NSGA-II. *IEEE Trans. Evol. Comput.* **2002**, *8*, 182–197. [CrossRef]
22. Li, H.; Love, P.E.D.; Drew, D.S. Effects of Overtime Work and Additional Resources on Project Cost and Quality. *Eng. Constr. Archit. Manag.* **2000**, *7*, 211–220. [CrossRef]
23. Mawdesley, M.J.; Al-jibouri, S.H.; Yang, H. Genetic Algorithms for Construction Site Layout in Project Planning. *J. Constr. Eng. Manag.* **2002**, *128*, 418–426. [CrossRef]

24. Kennedy, J.; Eberhart, R. Particle Swarm Optimization. In Proceedings of the IEEE International Conference on Neural Networks, Perth, Australia, 27 November–1 December 1995; Volume 4.
25. Kirkpatrick, S.; Gelatt, C.D., Jr.; Vecchi, M.P. Optimization by Simulated Annealing. *Science* **1983**, *220*, 671–680. [CrossRef] [PubMed]
26. Sacks, R.; Lee, G.; Teicholz, P.M. *BIM Handbook: A Guide to Building Information Modeling for Owners, Designers, Engineers, Contractors, and Facility Managers*; Wiley: Hoboken, NJ, USA, 2018.
27. Wang, J.; Zhang, X.; Shou, W.; Wang, X.; Xu, B.; Kim, M.J.; Wu, P. A BIM-Based Approach for Automated Tower Crane Layout Planning. *Autom. Constr.* **2015**, *59*, 168–178. [CrossRef]
28. Boje, C.; Guerriero, A.; Kubicki, S.; Rezgui, Y. Towards a Semantic Construction Digital Twin: Directions for Future Research. *Autom. Constr.* **2020**, *114*, 103179. [CrossRef]
29. Toth, P.; Vigo, D. *Vehicle Routing: Problems, Methods, and Applications*; MOS-SIAM Series on Optimization; Society for Industrial and Applied Mathematics SIAM: Philadelphia, PA, USA, 2014.
30. LaValle, S.M. *Planning Algorithms*; Cambridge University Press-University of Illinois, Urbana-Champaign: Champaign, IL, USA, 2006.
31. Gwak, H.-S.; Lee, H.-C.; Choi, B.-Y.; Mi, Y. GA-Based Optimization Method for Mobile Crane Repositioning Route Planning. *Appl. Sci.* **2021**, *11*, 6010. [CrossRef]
32. Hozjan, M.; Klanšek, U. Optimal Positioning of Mobile Cranes on Construction Sites Using Nonlinear Programming with Discontinuous Derivatives. *Sustainability* **2023**, *15*, 16889. [CrossRef]
33. Zhou, C.; Dai, F.; Xiao, Z.; Liu, W. Location Optimization of Tower Cranes on High-Rise Modular Housing Projects. *Buildings* **2023**, *13*, 115. [CrossRef]
34. Hasan, M.; Lu, M. Optimized Crane Mat Design and Transit Path Planning Using a Graph Search Algorithm. *Autom. Constr.* **2025**, *173*, 106107. [CrossRef]
35. Yao, G.; Li, R.; Yang, Y. An Improved Multi-Objective Optimization and Decision-Making Method on Construction Sites Layout of Prefabricated Buildings. *Sustainability* **2023**, *15*, 6279. [CrossRef]
36. Lei, J.; Zhang, Y.; Chen, Y.; Zhao, J.; Ren, W. A Multiobjective Construction Site Layout and Safety Planning Model Based on Evolutionary Algorithms. *Eng. Appl. Artif. Intell.* **2026**, *164*, 113177. [CrossRef]

Disclaimer/Publisher's Note: The statements, opinions and data contained in all publications are solely those of the individual author(s) and contributor(s) and not of MDPI and/or the editor(s). MDPI and/or the editor(s) disclaim responsibility for any injury to people or property resulting from any ideas, methods, instructions or products referred to in the content.